Deciphering the Preeclampsia-Specific Immune Microenvironment: The Role of Pro-inflammatory Macrophages

Haiyi Fei[#1,2,3], Xiaowen Lu [#1,2,3], Zhan Shi[#1,2,3], Xiu Liu[1,2,3], Cuiyu Yang[1,2,3], Xiaohong Zhu[4], Yuhan Lin[1,2,3], Ziqun Jiang[1,2,3], Jianmin Wang[1,2,3], Dong Huang[1,2,3], Liu Liu[1,2,3], Songying Zhang*[1,2,3]，Lingling Jiang*[1,2,3]

[1]Assisted Reproduction Unit, Department of Obstetrics and Gynecology, Sir Run Run Shaw Hospital, School of Medicine, Zhejiang University, Hangzhou, 310016, China.

[2]Zhejiang Provincial Clinical Research Center for Reproductive Health and Disease, Hangzhou, 310016, China.

[3]Zhejiang Key Laboratory of Precise Protection and Promotion of Fertility, Hangzhou, 310016, China.

[4]Department of Obstetrics and Gynecology, Zhejiang Xiaoshan Hospital, 310016, Hangzhou, China

***Co-corresponding authors**
Lingling Jiang
Assisted Reproduction Unit, Department of Obstetrics and Gynecology,
Sir Run Run Shaw Hospital, Zhejiang University School of Medicine,
310000, Hangzhou, China
E-mail: linglingjiang@zju.edu.cn

Songying Zhang
Assisted Reproduction Unit, Department of Obstetrics and Gynecology,
Sir Run Run Shaw Hospital, Zhejiang University School of Medicine,
310000, Hangzhou, China
E-mail: zhangsongying@zju.edu.cn

Abstract

Preeclampsia (PE), a major cause of maternal and perinatal mortality with highly heterogeneous causes and symptoms, is usually complicated by gestational diabetes mellitus (GDM). However, a comprehensive understanding of the immune microenvironment in the placenta of PE and the differences between PE and GDM is still lacking. In this study, Cytometry by time of flight (CyTOF) indicated that the frequencies of memory-like Th17 cells ($CD45RA^{-}CCR7^{+}IL\text{-}17A^{+}CD4^{+}$), memory-like $CD8^{+}$ T cells ($CD38^{+}CXCR3^{-}CCR7^{+}Helios^{-}CD127^{-}CD8^{+}$) and pro-inflam Macs ($CD206^{-}CD163^{-}CD38^{mid}CD107a^{low}CD86^{mid}HLA\text{-}DR^{mid}CD14^{+}$) were increased, while the frequencies of anti-inflam Macs ($CD206^{+}CD163^{-}CD86^{mid}CD33^{+}HLA\text{-}DR^{+}CD14^{+}$) and granulocyte myeloid-derived suppressor cells (gMDSCs, $CD11b^{+}CD15^{hi}HLA\text{-}DR^{low}$) were decreased in the placenta of PE compared with that of NP, but not in that of GDM or GDM&PE. The pro-inflam Macs were positively correlated with memory-like Th17 cells and memory-like

CD8$^+$ T cells but negatively correlated with gMDSCs. Single-cell RNA sequencing revealed that transferring the F4/80$^+$CD206$^-$ pro-inflam Macs with a Folr2$^+$Ccl7$^+$Ccl8$^+$C1qa$^+$C1qb$^+$C1qc$^+$ phenotype from the uterus of PE mice to normal pregnant mice induced the production of memory-like IL-17a$^+$Rora$^+$Il1r1$^+$TNF$^+$Cxcr6$^+$S100a4$^+$CD44$^+$ Th17 cells via IGF1-IGF1R, which contributed to the development and recurrence of PE. Pro-inflam Macs also induced the production of memory-like CD8$^+$ T cells but inhibited the production of Ly6g$^+$S100a8$^+$S100a9$^+$Retnlg$^+$Wfdc21$^+$ gMDSCs at the maternal-fetal interface, leading to PE-like symptoms in mice. In conclusion, this study revealed the PE-specific immune cell network, which was regulated by pro-inflam Macs, providing new ideas about the pathogenesis of PE.

Introduction

In recent years, low fertility is a global problem (Agbaglo et al., 2022), exacerbated by pregnancy complications. Preeclampsia (PE) is a progressive systemic disease during pregnancy, with pregnancy-induced hypertension, proteinuria, and liver and kidney injury as the main diagnostic indicators (Chappell et al., 2021). With a global prevalence of 7–10%, PE is a major cause of maternal and perinatal mortality and morbidity, especially in low-income and middle-income countries. The only specific treatment is delivery (Chappell et al., 2021). However, due to the variety of symptoms and the heterogeneity of the disease, the pathogenesis of PE is still unclear (Burton et al., 2019; Grotegut, 2016).

PE is often complicated by gestational diabetes mellitus (GDM), which is characterized by insulin resistance and associated with aberrant maternal immune cell adaption (Corrêa-Silva et al., 2018; McElwain et al., 2021; McIntyre et al., 2019). Studies have shown that GDM is an independent risk factor for preeclampsia (Nerenberg et al., 2013; Ostlund et al., 2004; Schneider et al., 2012). However, whether a different pathogenesis underlies between PE and GDM is still unclear.

The fetus is equivalent to a semi-homogenous graft for the mother. Therefore, maternal-fetal immune tolerance plays an important role in the maintenance of pregnancy. Currently, the pivotal mechanism underpinning the pathogenesis of preeclampsia is widely acknowledged to involve an increased frequency of pro-inflammatory M1-like maternal macrophages (Faas et al., 2014; Yao et al., 2019), along with an elevation in granulocytes that capable of superoxide generation (Lampé et al., 2011; D. Liu et al., 2021), CD56$^+$ CD94$^+$ natural killer (NK) cells (Bachmayer et al., 2006; Travis et al., 2020), CD19$^+$CD5$^+$ B1 lymphocytes (Jensen et al., 2012; LaMarca et al., 2011; Zhong et al., 2007), and activated γδ T cells (Chatterjee et al., 2017). Conversely, this pathological process is accompanied by a notable decrease in the frequency of anti-inflammatory M2-like macrophages (Faas et al., 2014; Yao et al., 2019) and NKp46$^+$ NK cells (Fukui et al., 2011). Adaptive immune response is also critical for the pathogenesis of PE (Deer et al., 2023). In PE, CD4$^+$ T cells prefer to differentiate into pro-inflammatory Th1 and Th17 (Eghbal-Fard et al., 2019; Fu et al., 2014; Lang et al., 2021; Lu et al., 2020; Saito et al. 2007) instead of non-inflammatory Th2 and Treg (Care et al., 2018; Cornelius et al., 2015a; Saito et al., 2007; Santner-Nanan et al., 2009; Sasaki et al., 2007).

Moreover, PE can be subdivided into early- and late-onset PE diagnosed before 34

weeks or from 34 weeks of gestation, respectively. Research has revealed that among the myriad of cellular alterations in PE, pro-inflammatory M1-like macrophages and intrauterine B1 cells display an augmented presence at the maternal-fetal interface of both early-onset and late-onset PE patients. Decidual natural killer (dNK) cells and neutrophils emerge as paramount contributors, playing a more crucial role in the pathogenesis of early-onset PE (Aneman I et al., 2020). However, a comprehensive and in-depth understanding of the maternal-fetal interface of PE is still lacking.

The immune cells crosstalk with each other at the maternal-fetal interface elaborately. For example, the interaction between B2 cells and Th cells depends on CD40 and its ligand CD40L, which helps B2 cells provide AT1-AAs and differentiate into memory B cells in reducing uterine perfusion pressure (RUPP) rats (Cornelius et al., 2015b). The cytokines derived from NK cells can promote the differentiation of Th17 to co-work in recurrent miscarriage (Fu et al., 2013). The intricate interplay and precise coordination between immune cells are pivotal in maintaining pregnancy. Nevertheless, the regulation of the immune network at the maternal-fetal interface of PE patients still needs to be further studied.

In this study, we combined cytometry by time of flight (CyTOF), single-cell RNA sequencing (scRNA-seq), and rodent experiment to identify the overall immune cell composition and their interactions at the maternal-fetal interface in PE, GDM, and GDM complicated with PE (GDM&PE). This study revealed the PE-specific immune cell network, which was regulated by pro-inflammatory macrophages, providing new ideas about the pathogenesis of PE.

Results

Overall immune cell profile in the placenta of PE, GDM, and GDM&PE

To fully characterize the immune microenvironment at the maternal-fetal interface of PE, we collected full-term placentas of PE and normal pregnancy (NP), and did a CyTOF test (**Table 1**), which panel was shown in **Table 2**. Since PE is usually complicated by GDM, the subjects of GDM and GDM complicated with PE (GDM&PE) were also included. The experimental workflow for CyTOF is shown in the schematic diagram (**Figure 1A**). We found that in addition to the well-known macrophages and T cells, there are also γδ T cells, B cells, NK cells, granulocytes, dendritic cells (DCs), and myeloid-derived suppressor cells (MDSCs). An overall distribution of $CD45^+$ cell subsets in placenta as shown in the t-SNE maps (**Figure 1B**). There were no significant differences in the proportion of these large subpopulations comparing the PE, GDM, GDM&PE group to the NP group (**Figure 1C**). To identify the ten cell subpopulations, CD4, CD8, and γδTCR were used as markers to distinguish $CD4^+$ T cells, $CD8^+$ T cells, and γδ T cells. CD11b is a marker that distinguishes myeloid cells, including macrophages and granulocytes (**Figure 1D**). The ten cell subsets were further annotated by 41 markers in the heatmap (**Figure 1E, Table 3**).

Specific altered T cell profile in the placenta of PE

To gain a comprehensive understanding of the distribution patterns within each cellular subset, we conducted separate clustering analyses for $CD4^+$T, $CD8^+$T, and γδT cells, respectively. We first analyzed 15 clusters of $CD4^+$ T cells from the placentas of NP, PE, GDM, and GDM&PE (**Figure 2A**). $CD4^+$ T cell clusters were defined by canonical marker set

signatures (**Figure 2-figure supplement 1A**). The frequencies of memory-like CD45RA$^-$CCR7$^+$CD69$^-$CD127^{low}TIGIT$^-$Helios$^-$ CD4$^+$ T ells (cluster 8) were significantly increased in individuals with PE compared with NP controls. At the same time, there was no significance in the GDM and GDM&PE groups compared with the NP group (**Figure 2B, Table 4**). We analyzed the expression of common intracellular molecules in CD4$^+$ memory-like T cells by sorting CD45RO$^+$CCR7$^+$CD4$^+$ T cells from placental samples by flow cytometry. Higher levels of IL-17A and lower levels of Foxp3 were found in memory-like CD45RO$^+$CCR7$^+$CD4$^+$ T cells in the placentas of individuals with PE (**Figure 2C**). Consistent with the results of CyTOF, higher fluorescence intensity of CD45RO$^+$CD4$^+$ T cells was found in the placentas of individuals with PE than that of NP, and this cell population was mainly located in the placental sinusoids (**Figure 2D**), suggesting that these T cells should be recently recruited. Moreover, lower expression of immune checkpoint molecules including T-cell immunoglobulin mucin-3 (Tim-3) and programmed cell death 1 (PD-1) was found in CD45RA$^-$CCR7$^+$CD4$^+$ memory T cells in the PE group, suggesting that these cells have a lower immunosuppressive capacity (Chen et al., 2022; Fanelli et al., 2021; Rasmussen et al., 2022; Wang et al., 2016), there was no significant difference in the GDM or GDM&PE groups comparing with the NP group (**Figure 2E**). Then, 18 clusters of CD8$^+$ T cells were analyzed (**Figure 2F**). CD8$^+$ T cell clusters annotation was based on the expression of canonical marker signatures (**Figure 2-figure supplement 1B**). CD38$^+$CXCR3$^-$CCR7$^+$Helios$^-$CD127$^-$ (cluster 2) memory-like CD8$^+$ T cells were significantly increased in the PE group (**Figure 2G, Table 4**).CD38$^+$CXCR3$^-$CCR7$^+$Helios$^-$CD127$^-$ memory-like CD8$^+$ T cells of the PE group expressed lower levels of PD-1 and TIGIT, suggesting the activation of cytotoxicity of these cells (**Figure 2H**) (Morita et al., 2020). Then, 22 clusters of γδT cells were analyzed and annotated (**Figure 2-figure supplement 1C-D**). Cluster 15 (Helios^{mid}CD28^{mid}CD69^{mid}HLA-DR^{mid}CD127^{mid}γδT cells), with lower expression of Tim3, was significantly decreased in the PE group (**Figure 2-figure supplement 1E-F**). Nevertheless, neither the CD4$^+$ T cells nor the CD8$^+$ T cells exhibited any alteration in the memory-like clusters when comparing the GDM or GDM&PE groups to the NP group.

In conclusion, significant changes in placental T cell profile were found in the placentas of PE but not in those of GDM or GDM&PE, suggesting that abnormal activation of T cells in the placenta is associated with the pathogenesis of PE.

Abnormal polarization of macrophages was correlated with specific immune cell subsets in individuals with PE

Except for T cells, we also analyzed 29 clusters of CD45$^+$CD3$^-$CD11b$^+$ cells from placentas of NP, PE, GDM, and GDM&PE, including 9 clusters of macrophages, 11 clusters of granulocytes, and 5 clusters of NK/NK-like cells (**Figure 3A**). The clusters of CD45$^+$CD3$^-$CD11b$^+$ cells were defined by canonical marker set signatures (**Figure 3B**). Moreover, significantly decreased frequencies of CD68^{mid}CD39^{mid}HLA-DR^{low}CD11b$^+$CD15$^+$ granulocytes (cluster 12), which are identified as granulocyte myeloid-derived suppressor cells (gMDSCs), were found in the PE group (**Figure 3C, Table 4**). In addition, the frequency of anti-inflammatory macrophages (anti-inflam Macs) (CD206$^+$CD163$^-$CD86^{mid}CD33$^+$HLA-DR$^+$, cluster 25) was also significantly decreased, whereas the frequency of pro-inflammatory macrophages (pro-inflam Macs) (CD206$^-$CD163$^-$CD38^{mid}CD107a^{low}CD86^{mid}HLA-DR^{mid}CD14$^+$, cluster 23) was significantly increased in the PE group (**Figure 3C, Table 4**). However, the

172 frequencies of macrophages and gMDSCs were unchanged significantly in the GDM or
173 GDM&PE groups.
174 Pearson correlation analysis indicated positive correlations between pro-inflam Macs
175 (cluster 23 in $CD11b^+$ cells) and $CD4^+$ memory-like T cells (cluster 8 of $CD4^+$ T cells), as well as
176 $CD8^+$ memory-like T cells (cluster 2 in $CD8^+$ T cells). $CD206^-$ pro-inflam Macs were negatively
177 correlated with gMDSCs (cluster 12 in $CD11b^+$ cells), but were not statistically significant.
178 Conversely, $CD206^+$ anti-inflam Macs (cluster 25 in $CD11b^+$ cells) were positively correlated
179 with gMDSCs and negatively correlated with $CD8^+$ memory-like T cells (**Figure 3D, 3E**).
180 These results suggested that abnormally polarized $CD206^-$ pro-inflam Macs are positively
181 correlated with memory-like $CD4^+$ and $CD8^+$ T cells in the placentas of individuals with PE and
182 negatively correlated with gMDSCs.
183 **$F4/80^+CD206^-$ pro-inflam Macs induced immune imbalance at the maternal-fetal**
184 **interface and PE-like symptoms**
185 Though increased pro-inflam Macs have been reported in the placenta from individuals
186 with PE (Faas et al., 2014), few studies have reported the interaction between macrophages
187 and other immune cells in the placenta. In this study, transcriptome RNA-seq was used to
188 analyze the difference between $CD45^+F4/80^+CD206^-$ pro-inflam Macs and
189 $CD45^+F4/80^+CD206^+$ anti-inflam Mac isolated from the uterus and placentas of mice with
190 reducing uterine perfusion pressure (RUPP) (**Figure 4A**). The diagrammatic representation of
191 the RUPP model is presented in Figure 4-figure supplement 1A. To establish the PE mouse
192 model, we ligated uterine arteries in pregnant mice on day 12.5 of gestation, and mice with
193 sham operation were considered as controls (**Figure 4-figure supplement 1A**). We found that
194 mice of RUPP showed an increased embryo absorption rate, decreased fetal weight, and pup
195 crown-rump length compared with the sham operation group (**Figure 4-figure supplement**
196 **1B**). Increased systolic blood pressure (SBP) and urine albumin creatine ratio (UACR) were
197 also observed in mice with RUPP, which indicated a successful PE mice mode was built
198 (**Figure 4-figure supplement 1C**). Then, we injected the PE-mice derived macrophages into
199 normal pregnant mice. An increased embryo resorption rate, decreased fetal top-rump length
200 and fetal weight were found in mice injected with PE-mice derived macrophages compared
201 with mice injected PBS (**Figure 4-figure supplement 1D**). Increased SBP and UACR were
202 also found in mice injected with PE-mice derived macrophages (**Figure 4-figure supplement**
203 **1E**).
204 In addition, the green fluorescent protein (GFP) pregnant mice were used to distinguish
205 between maternal and fetal derived macrophages. The wild-type (WT) female mice were
206 mated with either transgenic male mice, genetically modified to express GFP to generate
207 either GFP-expressing pups (GFP^+pups), or mated with WT male mice for control (**Figure**
208 **4-figure supplement 1F**). We found that the majority of macrophages in the uterus and
209 placenta are of maternal origin ($CD11b^+GFP^-$). In contrast, fetal-derived macrophages
210 ($CD11b^+GFP^+$) represent a mere fraction of the total macrophage population (**Figure 4-figure**
211 **supplement 1G**). In light of these findings, we have incorporated mouse uterine tissues to
212 isolate macrophages for subsequent experiments with enhanced effectiveness.
213 Significant differences were found between the pro-inflam and anti-inflam macrophages
214 derived from RUPP mouse (**Figure 4B**). There are 2123 genes increased, and 2699 genes
215 decreased significantly in the pro-inflam Macs compared to the anti-inflam Macs (**Figure 4C**).

The expression levels of genes associated with inflammatory response (Ccl7, Ccl8, Ccl2, IL6) (He et al., 2019; Wu et al., 2023), complement system activation (C1qa, C1qb) (Chen et al., 2021), and lipid metabolism (Pltp, Apoe) (Desrumaux et al., 2016) were significantly increased in the pro-inflam Macs; whereas the expression levels of genes associated with the regulation of angiogenesis and vascular endothelial growth factor production (VEGFα, Macro) and tissue development (TGF-β1, Thbs1, Fn1, Slpi) (Jin et al., 2023; Nugteren et al., 2021; Li et al., 2022) were significantly decreased (**Figure 4C, 4D**). Moreover, Gene Set Enrichment Analysis (GSEA) was performed to explore the most significantly enriched functional terms between the two groups of macrophages. We found that NF-κB signaling and interspecies interaction between organisms were enriched in the pro-inflam Macs, while tissue development and epithelial cell morphogenesis were enriched in the anti-inflam Macs (**Figure 4E**).

To further investigate the effect of the pro-inflam Macs in immune imbalance at the maternal-fetal interface, PLX3397, the inhibitor of CSF1R, which is needed for macrophage development, was used to deplete the macrophages of pregnant mice (X. Chen et al., 2023; J. Chen et al., 2022) (**Figure 4-figure supplement 2A**). As expected, an increased embryo resorption rate, decreased fetal top-rump length and fetal weight were found in mice injected with pro-inflam Macs (**Figure 4F**). Increased SBP and UACR were also found in mice injected with pro-inflam Macs (**Figure 4G**). Moreover, it is shown that $CD44^+$ memory-like Th17 cells and memory-like $CD8^+$ T cells increased while $CD11b^+Ly6G^+$ gMDSCs decreased in mice injected pro-inflam Macs compared with mice injected anti-inflam Macs, which validated our findings with CyTOF (**Figure 4H**). Clodronate liposomes were also used to deplete the macrophages of pregnant mice (X. Liu et al., 2022) before pro-inflam Macs or anti-inflam Macs were injected into the mice. The same experimental results were obtained (**Figure 4-figure supplement 2B-2E**). In conclusion, the $F4/80^+CD206^-$ pro-inflam Macs induced immune imbalance at the maternal-fetal interface and PE-like symptoms.

Pro-inflam Macs and anti-inflam Macs subsets are phenotypically heterogeneous

To further explore the role that macrophages play in the immune imbalance at the maternal-fetal interface in PE, scRNA-seq was performed to analyze the $CD45^+$ immune cells in the uterus and placenta from mice that were injected with pro-inflam Macs or anti-inflam Macs from the uterus and placentas of RUPP mice. An unsupervised cluster detection algorithm (SEURAT) was applied and eight types of immune cells were detected by mostly distinguishable cell type-specific genes, including macrophages, monocytes, granulocytes, T/NK cells, B cells, DC-like cells, mast cells, and basophils (**Figure 5A, 5B**). Macrophages were further identified into 15 clusters defined by marker set signatures. Single-cell differential expression analysis (SCDE) was performed for each population and characteristic gene expression patterns were detected for cluster 0-cluster 14 to characterize the phenotypes of these subsets in detail (**Figure 5C, Figure 5-figure supplement 1C**). We found that the frequency of cluster 0 was significantly increased in mice injected with pro-inflam Macs, while the frequency of cluster 1 was significantly decreased (**Figure 5D**). We also found that cluster 0 highly expresses genes associated with fetal and tissue resident (Folr2) (Nalio et al., 2022; Thomas et al., 2021), complement system activation (C1qa, C1qb, C1qc) (Chen et al., 2021), and inflammatory response (Ccl7, Ccl8) (He et al., 2019; Wu et al., 2023); while cluster 1 highly expresses genes associated with tissue repair (Chil3, Slpi, Fn1) (Jin et al., 2023; Nugteren et al., 2021; Li et al., 2022), blood vessel morphogenesis (Thbs1) (Che et al., 2021)

and preventing oxidative stress (Gsr, Mgst1) (Coppo et al., 2022) (**Figure 5E**). Changes in gene expression patterns of cluster 0 (pro-inflam Macs) and cluster 1 (anti-inflam Macs) were analyzed in mice injected the pro-inflam Macs or anti-inflam Macs. We found that enriched GO terms in cluster 0 and cluster1 including 'antigen processing and presentation of exogenous antigen' and 'inflammatory response' in the pro-inflam Macs group (**Figure 5F**), in which high expression of genes such as CCL5, CCL8, CALR, IRF7, IL10, IFI44, IFI30, OAS3, etc. could be observed (**Figure 5G**). The control group showed elevated expression of MMP14, Chil3, EGR1, ATF3 and VASP (**Figure 5G**); and these genes were enriched in 'vascular endothelial growth factor production' and 'tissue development' (**Figure 5F**). These results were consistent with the transcriptome RNA sequencing results of macrophages.

These data suggested that the $CD45^{+}F4/80^{+}CD206^{-}$ pro-inflam Macs with a $Folr2^{+}Ccl7^{+}Ccl8^{+}C1qa^{+}C1qb^{+}C1qc^{+}$ phenotype play an important role in the development of PE.

Pro-inflam Macs induced the memory-like Th17 cells, which was associated with the development and recurrence of PE

We also analyzed the scRNA-seq data of uterine T/NK cells from mice that were injected with or without pro-inflam Macs. T/NK cells were further identified into 12 clusters defined by marker set signatures (**Figure 6A, Figure 6-figure supplement 1A**). We found that the frequency of cluster 0 was increased in mice injected with pro-inflam Macs, while the frequency of cluster 1 and cluster 2 were significantly decreased (**Figure 6B**). In addition to genes associated with Th17 cells (IL-17a, IL17f, Rora, Il1r1, TNF) (Wu et al., 2019; Leite et al., 2023), cluster 0 also exhibits high expression of genes associated with memory phenotype (Cxcr6, S100a4, CD44) (Schroeder et al., 2023; Bieberich et al., 2021), suggesting that cluster 0 was the memory-like Th17 cells (**Figure 6C**). Cluster 1 exhibited high expression of genes associated with immunoregulation (Lef1, Tcf7, Ccr7) (Qiu et al., 2022; Sekine et al., 2020); Cluster 2 exhibited high expression of genes associated with immunomodulation (Gata3, GITR, CD28), suggesting that cluster 1 and 2 were T cells with immunomodulation function (Esensten et al., 2016; Pai et al., 2023) (**Figure 6-figure supplement 1B)**. Changes in gene expression patterns of cluster 0 (memory-like Th17 cells) were analyzed in the pro-inflam Macs group and control group. We found that in the pro-inflam Macs group, enriched GO terms including 'positive regulation of response to external stimulus' and 'tumor necrosis factor production' (**Figure 6D**), in which highly express genes such as TNFSF11, TNF, IL27RA, IGF1R, CD226, LAMP1 (**Figure 6E**). The control group showed elevated expression of ASS1, EIF5, S100A9, CTLA4, S100A8 and CXCR4 (**Figure 6E**); these genes were enriched in GO terms including 'regulation of programmed cell death' and 'cellular biosynthetic process' (**Figure 6D**). In summary, the pro-inflam Macs induced memory-like Th17 cells, which were characterized by $IL\text{-}17a^{+}IL17f^{+}Rora^{+}Il1r1^{+}TNF^{+}Cxcr6^{+}S100a4^{+}CD44^{+}$.

To confirm the importance of memory-like $CD4^{+}$ T cells in the pathogenesis of PE, the $CD4^{+}CD44^{+}$ T cells in the uterus and placentas from RUPP or NP mice were sorted and intravenously injected into normal pregnant mice on day12.5 of gestation (**Figure 6F**). The $CD4^{+}CD44^{+}$ T cells derived from RUPP mouse were characterized by an increased frequency of Th17 cells and a reduced frequency of Tregs (**Figure 6F**). Increased embryo absorption rate, decreased fetal weight and pup crown-rump length were found in mice injected with PE mouse-derived $CD4^{+}CD44^{+}$ T cells (**Figure 6G**). The PE-like symptoms, including increased

304 SBP and UACR, were also observed in those mice (**Figure 6H**).

305 It has been reported that sustained expansion of immunosuppressive memory Tregs
306 during prior pregnancy is beneficial for maintaining a second pregnancy (Rowe et al., 2012). To
307 verify whether memory-like Th17 cells promote the recurrence of PE, we established a second
308 pregnant mouse model with a history of PE or NP in the first pregnancy. An increased embryo
309 resorption rate, decreased crown-rump length, and fetal weight were found in mice with a
310 history of PE pregnancy compared with those with a history of NP pregnancy (**Figure 6-figure**
311 **supplement 1C**). Moreover, mice with a history of PE in the first pregnancy showed increased
312 SBP and UACR during the second pregnancy (**Figure 6-figure supplement 1D**). Consistently,
313 higher levels of IL-17A were also found in memory-like $CD4^+$ T cells in mice with a history of PE
314 in the first pregnancy (**Figure 6-figure supplement 1E**).

315 The uterine granulocytes from mice that were transferred with pro-inflam Macs from PE
316 mice were also analyzed using scRNA-seq. Granulocytes were identified into 12 clusters
317 defined by marker set signatures (**Figure 6-figure supplement 2A, 2B**). We found that the
318 frequency of cluster 3 were decreased (**Figure 6-figure supplement 2A**)).And cluster 3 highly
319 expressed gMDSCs associated genes (Ly6g, S100a8, Retnlg, Wfdc21) (von Wulffen et al.,
320 2023; Kao al., 2023) (**Figure 6-figure supplement 2C**).-Changes in gene expression patterns
321 of cluster 3 (gMDSCs) were analyzed in the pro-inflam Macs group and the control group.
322 Enriched GO terms including 'tumor necrosis factor production' and 'leukocyte mediated
323 immunity' were found in the pro-inflam Macs group (**Figure 6-figure supplement 2E**), which
324 highly express the genes such as IRF7, EGR1, C1QA, C1QB, CCL2, CSF3R, TNFRSF1B
325 (**Figure 6-figure supplement 2D**). Except for gMDSCs, we also revealed a pronounced
326 increase in the proportion of $CD15^+CD66b^+$ neutrophils among PE patients, implying the
327 importance of neutrophils in the development of PE (Akkari L et al., 2024) (**Figure 6-figure**
328 **supplement 2F**).

329 In conclusion, pro-inflam Macs could induced the differentiation of
330 $IL\text{-}17a^+IL17f^+Rora^+Il1r1^+TNF^+Cxcr6^+S100a4^+CD44^+$ memory-like Th17 cells, which was
331 associated with the development and recurrence of PE. And the pro-inflam Macs also
332 suppressed the production of $Ly6g^+S100a8^+Retnlg^+Wfdc21^+$ gMDSCs.

333 **Pro-inflam Macs induced the production of memory-like Th17 cells via IGF1-IGF1R**

334 Our results above showed that pro-inflam Macs induced memory-like Th17 cells in PE,
335 however, the underlying molecular mechanisms were still unknown. CellPhoneDB analysis
336 indicated that increased communication counts and signaling pathways numbers between
337 macrophages and T/NK cells were observed in mice injected with pro-inflam Macs (**Figure**
338 **7—figure supplement 1A, 1B**). Then we identified the interacting ligand-receptor pairs
339 between different types of immune cells and macrophages. Insulin-like growth factor 1 (IGF1)
340 -IGF1 receptor (IGF1R) ligand-receptor pair was significantly enhanced between
341 macrophages and T/NK cells in mice injected with pro-inflam Macs (**Figure 7A**). IGF1 has
342 significant effects on immune function maintenance, and signaling through IGF1R could cause
343 increased aerobic glycolysis, favoring Th17 cell differentiation over that of Treg cells
344 (Bekkering et al., 2018; DiToro et al., 2020). For further demonstration, we analyzed the
345 frequencies of $IGF1^+CD14^+$ cells and $IGF1R^+CD4^+$ cells in placentas of individuals with PE and
346 NP and found both of these two cells were significantly increased in the PE group (**Figure 7B**).

347 Trophoblast-derived extracellular vesicles from the placenta of PE (PE-EVs), which carry

348 the fetal antigen, could induce M1-like macrophage (pro-inflammatory Macs) polarization to
349 participate in the development of PE according to our previous study (X. Liu et al., 2022). To
350 confirm whether pro-inflammatory Macs induced the production of memory-like Th17 cells via
351 IGF1-IGF1R, macrophages from human peripheral blood, after incubating with PBS,
352 trophoblast-derived extracellular vesicles from NP (NP-EVs) or PE-EVs in vitro, were
353 co-cultured with $CD4^+$ naïve T cells (**Figure 7C**). The frequencies of memory-like $CD45RO^+$
354 $CCR7^+$ $IL\text{-}17A^+$ $CD4^+$ cells significantly increased in the PE-EVs-induced macrophages group
355 rather than in the NP-EVs-induced macrophages group. However, the frequencies of
356 memory-like Th17 cells significantly decreased after $CD4^+$ naïve T cells were treated with the
357 IGF1R inhibitor BMS-754807 (**Figure 7D**).
358 To investigate the role of IGF1-IGF1R in the development of PE in vivo, $CD45^+CD4^+$ T
359 cells from NP mice were isolated and treated with BMS-754807 or PBS, then injected into NP
360 mice at day 11.5 of gestation (**Figure 7E**). Lipopolysaccharide (LPS)-induced PE mice model
361 was constructed by intraperitoneal injection of LPS on day12.5 and day15.5 of gestation (Han
362 et al., 2021), and an anti-CD4 antibody was used to deplete the $CD4^+$ T cells in pregnant mice.
363 The mice injected with $CD4^+$ T cells treated by BMS-754807 presented decreased embryo
364 resorption rate and increased pup crown-rump length and fetal weight (**Figure 7F**), decreased
365 SBP and UACR (**Figure 7G**), and decreased frequency of memory-like Th17 cells at the
366 maternal-fetal interface (**Figure 7H**). These data suggested that pro-inflam Macs could induce
367 the production of memory-like Th17 via the IGF1-IGF1R, leading to the development of PE.

368 **Discussion**

369 Preeclampsia, a progressive systemic disease during pregnancy, is closely related to the
370 alterations in the immune environment at the maternal-fetal interface. In this study, the overall
371 immune cell profiles in the placenta of individuals with NP, PE, GDM and GDM&PE were
372 detected by CyTOF and a PE-specific change in immune microenvironment of maternal-fetal
373 interface was described for the first time. Further, we provided a novel insight that pro-inflam
374 Macs induced memory-like Th17 cells, memory-like $CD8^+$ T cells, and suppressed the
375 production of gMDSCs in mice maternal-fetal interface by scRNA-seq. In addition, we first
376 validated that IGF1-IGF1R was involved in producing memory-like Th17 cells induced by
377 pro-inflam Macs in vitro and in vivo, thus leading to the development of PE.
378 Various studies represented the effect of a single subset of immune cells in the
379 pathogenesis of PE or GDM (Bachmayer et al., 2006; Care et al., 2018; Cornelius et al., 2015a;
380 Eghbal-Fard et al., 2019; Faas et al., 2014; Fu et al., 2014; Fukui et al., 2011; Lampé et al.,
381 2015; Lampé et al., 2011; Lang et al., 2021; D. Liu et al., 2021; Lu et al., 2020; Santner-Nanan
382 et al., 2009; Sasaki et al., 2007; Travis et al., 2020; Yao et al., 2019). Miller et al. provided an
383 overall analysis of immune cells in the human placental villi in the presence and absence of
384 spontaneous labor at term by scRNA-seq (Miller et al., 2022). Fangyuan Luo et al. unveiled the
385 intricate interplay existing between $SPP1^+$M1 cells and the $IGFBP1^+SPP1^+$ extracellular villous
386 trophoblast in the context of PE by using sc-RNA seq (Luo F et al., 2023). Li Y et al. highlighted
387 a key role of a distinct perivascular inflammatory $CD11c^{high}$ decidual macrophages
388 subpopulation in the pathogenesis of preeclampsia through sc-RNA sequencing (Li Y et al.,
389 2024). However, The immune cells crosstalk with each other at the maternal-fetal interface
390 elaborately. A comprehensive and in-depth understanding of the immune microenvironment at
391 the maternal-fetal interface of PE is still lacking. Here, we used CyTOF and scRNA-seq to

392 comprehensively analyze the immune cell profile and explore the interaction of immune cells in
393 PE. Additionally, most previous studies have reported immune cells from maternal systemic
394 circulation rather than directly from the tissue of maternal-fetal interface (Cornelius et al.,
395 2015b; Deer et al., 2021; Santner-Nanan et al., 2009; Shields et al., 2018; Wallace et al.,
396 2012). In this study, cells were directly isolated from the tissue of maternal-fetal interface,
397 which is considered as a more accurate approach to unveil the real immune environment of
398 the maternal-fetal interface.

399 Abnormal inflammatory responses were reported to play an important role in the
400 pathogenesis of both PE and GDM (Aneman et al., 2020; Corrêa-Silva et al., 2018; Deer et al.,
401 2023; Jung et al., 2022; McElwain et al., 2021). However, it is unclear how the maternal-fetal
402 interface immune microenvironment differs between the two diseases. We analyzed the
403 overall placental immune cell profile in NP, PE, GDM and GDM&PE by CyTOF and revealed a
404 PE-specific immune cell profile: The frequencies of memory-like Th17 cells
405 ($CD45RA^{-}CCR7^{+}IL\text{-}17A^{+}CD4^{+}$), memory-like $CD8^{+}$ T cells
406 ($CD45RA^{-}CCR7^{+}CD38^{+}pAKT^{mid}CD127^{low}CD8^{+}$) and pro-inflam Macs
407 ($CD206^{-}CD163^{-}CD38^{mid}CD107a^{low}CD86^{mid}HLA\text{-}DR^{mid}CD14^{+}$) were increased, while the
408 decreased frequencies of $CD69^{hi}Helios^{mid}CD127^{mid}$ γδT cells, anti-inflam Macs
409 ($CD206^{+}CD163^{-}CD86^{mid}CD33^{+}HLA\text{-}DR^{+}CD14^{+}$) and granulocyte myeloid-derived suppressor
410 cells (gMDSCs, $CD11b^{+}CD15^{hi}HLA\text{-}DR^{low}$) were observed in the placenta of PE, but not in that
411 of GDM or GDM&PE compared with that of NP.

412 PE is often divided into two subtypes based on the time of onset. Late-onset PE, occurring
413 at 34 weeks of gestation or later, accounts for most preeclampsia cases, while early-onset PE,
414 occurring before or at 33 weeks of gestation (Lisonkova and Joseph, 2013). However, our
415 previous study observed no significant difference in the M1/M2 macrophage polarization in
416 placentas with early-onset or late-onset PE (X. Liu et al., 2022). Therefore, our research was
417 conducted regardless of the preeclampsia-onset type to ensure consistency in macrophage
418 polarization of the two subtypes.

419 There have been studies indicating that pro-inflammatory macrophages, Th17 cells and
420 $CD8^{+}$ T cells play an essential role in PE development (Care et al., 2018; Eghbal-Fard et al.,
421 2019; Lager et al., 2020; Yao et al., 2019). Macrophages was indicated with a
422 pro-inflammatory phenotype in the placenta with PE (Faas et al., 2014; Yao et al., 2019). Care
423 et al. reported that placental Tregs helped suppress inflammation at the maternal-fetal
424 interface (Care et al., 2018). Similarly, Lu et al. found an abnormal increase of IL-17A in the
425 placenta in the development of PE (Lu et al., 2020). Meanwhile, the abnormal infiltration of
426 $CD8^{+}$ T cells in the placenta may contribute to PE (Lager et al., 2020). Consistent with the
427 previous findings, we found that memory-like $CD4^{+}$ and memory-like $CD8^{+}$ T cells significantly
428 increased in the PE group and that IL-17A was significantly higher expressed in $CD4^{+}$
429 memory-like T cells from the PE group, which is vital in vascular inflammation, leading to the
430 development of PE (Amador et al., 2014; Madhur et al., 2021). Though memory T cells play a
431 key role in fetal-maternal tolerance in normal pregnancy (Kieffer et al., 2019), few studies have
432 reported the characteristics of memory-like T cells in the development of PE.

433 We constructed an adoptive transferred mouse model. The injection of $CD4^{+}$ T cells from
434 RUPP mouse, characterized by an increased frequency of Th17 cells and a reduced
435 frequency of Tregs, induced PE-like symptoms in pregnant mice. Tregs which are well known

436 to undergird maternal tolerance of the fetus, and which are well known to have an overlapping
437 developmental trajectory with RORgt$^+$ Th17 cells (Robertson SA et al., 2019; Sefik E et
438 al.,2015). This study underscores the importance of Th17/Treg cell balance in maintaining
439 pregnancy homeostasis. And it is worth noting that we isolated CD4$^+$ memory-like T cells
440 directly from the maternal-fetal interface, which is different from previous studies that the CD4$^+$
441 T cells for adoptive transfer were isolated from the spleen and induced in vitro (Cornelius et al.,
442 2015b; Deer et al., 2021; Shields et al., 2018; Wallace et al., 2012). Recurrence is an important
443 concern in individuals with PE (Bernardes et al., 2019). We found that a prior PE pregnancy
444 increased the probability of PE in the next pregnancy in mice, accompanied by an increased
445 frequency of memory-like Th17 cells at the maternal-fetal interface, suggesting that increased
446 memory-like Th17 cells are positively related to the recurrence of PE. However, further studies
447 are needed to confirm the function of the fetal-specific memory Th17 cells in the recurrence of
448 PE.
449 Activation of CD8$^+$ T cells and Th1 cells can be induced by abnormal polarized
450 macrophages in recurrent miscarriage (Li et al., 2022). The gMDSCs have been reported to
451 have immune suppressive activity and are necessary for maintaining maternal-fetal tolerance
452 (Köstlin-Gille et al., 2019; Zhou et al., 2018). However, the correlation between macrophages
453 and other immune cells in the development of PE remained unclear. We verified that
454 pro-inflam Macs induced memory-like Th17 cells and memory-like CD8$^+$ T cells and inhibited
455 the production of gMDSCs in PE by correlation analysis and adoptive transfer in animal
456 experiments for the first time, indicating that the immune cells orchestrate a network in the
457 maternal-fetal interface elaborately. However, PLX3397, used in this study, emerges as a
458 promising small-molecule compound, endowed with the capability to traverse the placental
459 barrier, thereby potentially influencing the development and function of fetal macrophages. In
460 addition to gMDSCs, we conducted immunofluorescence analysis of placental tissue,
461 specifically targeting CD66b^{high} neutrophils. Our findings revealed a pronounced increase in
462 the proportion of neutrophils among PE patients, fostering the hypothesis that IL-17A produced
463 by Th17 cells might orchestrate the migration of neutrophils towards the placental milieu. This
464 migratory response, in turn, could potentially trigger reactive oxygen species (ROS)-mediated
465 immunopathology, which subsequently lead to PE (Akkari L et al., 2024).
466 The function of IGR1 and IGF1R in PE is controversial. IGF1 plays a significant role in
467 maintaining immune function, and IGF1R facilitates the differentiation of naïve CD4$^+$ T cells
468 into Th17 cells (DiToro et al., 2020). A study showed that IGF-1R was downregulated in the
469 serum of individuals with PE (Liao et al., 2021). Decreased amounts of IGF1R were also found
470 in the placentas of individuals with PE (Robajac et al., 2015). However, another study found no
471 significance in the affinity and the number of IGF-1R between placentas from individuals with
472 PE or not (Díaz et al., 2005). We found that mice exhibiting PE symptoms had significantly
473 enhanced IGF1-IGF1R interaction between inflammatory macrophages and memory-like Th17
474 cells by analyzing the data of scRNA-seq. Then, this finding was further confirmed in human
475 placentas from individuals with PE and NP, for the frequencies of IGF1$^+$ CD14$^+$ cells and
476 IGF1R$^+$ CD4$^+$ cells were found to significantly increase in the PE group. In vitro, we found that
477 PE-EVs-treated macrophages secreted more IGF1 than NP-EV-treated macrophages and
478 induced a higher frequency of memory-like Th17 cells. The inhibition of IGF1R on CD4$^+$ naïve
479 T cells resulted in a decreased frequency of memory-like Th17 cells, implying that the

480 IGF1-IGF1R is critical for the production of memory-like Th17 cells induced by inflammatory
481 macrophages. Animal experiments confirmed that IGF1R inhibition on $CD4^+$ T cells at the
482 maternal-fetal interface reduced the frequency of memory-like Th17 cells and relieved PE-like
483 symptoms.
484 In addition, placentas from different groups for CyTOF analysis and flow cytometry were
485 matched by age, preterm pregnancies, and previous abortion history; however, there are
486 differences in body mass index (BMI), gestational age, term pregnancies, and the number of
487 living children. Obesity can increase inflammatory and oxidative stress markers in the
488 placental environment (Spradley et al., 2015). Also, it has been reported that the placental
489 immune state shifts with gestational age (Lewis et al., 2018). However, as PE is often
490 accompanied by obesity and early termination of pregnancy, it is difficult to exclude these
491 factors in sample collection. Moreover, limited placental samples in the GDM&PE group are
492 the shortage of this study, for it is hard to collect enough clean samples that exclude
493 interference factors because the number of pregnant women exposed to COVID-19 has
494 increased sharply since December 2022 in China.
495 In summary, this study demonstrated the statistically distinguished placental immune
496 microenvironment in individuals with PE, but not in those with GDM or GDM&PE. More
497 importantly, macrophages orchestrate a network in the maternal-fetal interface elaborately.
498 These findings provide novel insights into PE pathogenesis and a potential immune target for
499 the clinical prevention and treatment of PE.
500
501
502 **Materials and Methods**
503 **Clinical sample collection**
504 The samples used in this study were collected from Sir Run Run Shaw Hospital between
505 October 2020 and August 2023. Informed consent was obtained from all volunteers, and the
506 Ethics Committee of Sir Run Run Shaw Hospital, Zhejiang University School of Medicine,
507 approved the study. Human placentas were obtained from women with NP, PE, GDM, or
508 GDM&PE who underwent elective cesarean delivery. The diagnostic criteria for PE included
509 new-onset hypertension after 20 weeks of gestation with SBP ≥140 mmHg and/or diastolic
510 blood pressure ≥90 mmHg and proteinuria (≥300 mg) on at least two occasions. A positive
511 glucose tolerance test diagnoses gestational diabetes mellitus. Women with normal blood
512 pressure, full-term pregnancies, and no complications were designated as controls. The
513 detailed clinical characteristics of the pregnant women in this study are presented in Table 5
514 and Table 6.
515 **Mice**
516 Eight-week-old female C57 mice and ten-week-old male BALB/c mice were purchased
517 from Hangzhou Ziyuan Laboratory Animal Technology Co., Ltd (Hangzhou, China) and
518 Shanghai Jihui Experimental Animal Breeding Co., Ltd (Shanghai, China), respectively. All
519 animals were maintained under pathogen-free conditions. The Guide for the Care and Use of
520 Laboratory Animals (China) conducted all experimental procedures involving animals, and the
521 Animal Research Ethics Committee of the Sir Run Run Shaw Hospital of Zhejiang University
522 approved the protocols.
523 Female C57 mice were mated with male BALB/c mice to establish an allogeneic

524 pregnancy model (Rowe et al., 2012). The day of the vaginal plug detection was considered
525 day 0.5 of pregnancy. SBP was measured using a noninvasive mouse tailcuff BP analyzer
526 (BP-2010A, Softron, Japan) at 12.5, and 16.5 days of gestation. Three random urine samples
527 were collected after day 16.5 of gestation, and UACR was measured by urinary microalbumin
528 (CH0101060, Maccura, China). Mice were euthanized on day 18.5 of gestation.

529 **Reduction in uterine perfusion pressure mouse model**

530 To construct a mouse model of PE, we ligated uterine arteries in pregnant mice on day
531 12.5 of gestation. Briefly, after 4% chloral hydrate was intraperitoneally injected for anesthesia,
532 bilateral incisions were made on the back of the pregnant mice, and surgical sutures were
533 used to reduce the blood flow of the bilateral uterine arcades.

534 **Isolation of single cells from the mouse uterus and human placenta**

535 Uterus from pregnant mice and placentas from volunteers were washed twice with
536 ice-cold PBS and cut into small pieces. The tissues were digested with collagenase type IV (1
537 mg/ml, Sigma-Aldrich, USA) and DNase I (0.01 mg/ml, Sigma-Aldrich, U.S.A) in RPMI 1640
538 medium (Thermo Fisher Scientific) for 40 min at 200 rpm and 37 °C. The suspensions were
539 strained through 70-μm nylon mesh and centrifuged at 500×g for 5 minutes. Leaving the
540 supernatants, the cell pellets from human placentas need an extra purification by Ficoll (P4350,
541 Solarbio, China) according to the manufacturer's instructions. Human $CD4^+$ memory T cells
542 were isolated using a Human Central and Effector Memory $CD4^+$ T Cell Isolation Kit (17865,
543 STEMCELL, Canada).

544 **Adoptive transferred mouse model**

545 Endogenous macrophages or $CD4^+$ T cells were depleted by injecting PLX3397 (S7818,
546 Selleck, USA), clodronate liposomes (40337ES08, YEASEN, China) or anti-CD4 antibody
547 (BE0003-1, BioXcell, USA) intraperitoneally every three days starting from day 10.5 of
548 gestation.

549 For the adoptive transferred mouse model, phycoerythrin-conjugated anti-mouse CD4
550 (12-0041-82, eBioscience, USA) and Pc5.5-conjugated anti-mouse CD44 (45-0441-82,
551 eBioscience, USA) were used to label $CD4^+$ memory-like T cells from uterus and placentas.
552 PE-conjugated anti-mouse CD45 (E-AB-F1136D, Elabscience, China), FITC-conjugated
553 anti-mouse F4/80 (11-4801-82, eBioscience, USA), and PE-Cyanine7-conjugated anti-mouse
554 CD206 (141719, Biolegend, USA) were used to label anti-inflam Macs from uterus and
555 placentas, and the remaining $CD45^+F480^+CD206^-$ cells were considered pro-inflam Macs. The
556 MoFlo Astrios EQ FACS Cell Sorter at Core Facilities, ZheJiang University School of Medicine
557 (China), was used to obtain specific cells with a purity of > 96%. Briefly, 2–5 × 10^5 $CD4^+$ $CD44^+$
558 T cells, 5×10^5 pro-inflam Macs, or 5×10^5 anti-inflam Macs were injected to pregnant C57 mice
559 intravenously at day 12.5 of gestation.

560 2–5 × 10^5 $CD45^+CD4^+$ T cells from uterus and placentas of pregnant mice were sorted
561 and transferred to pregnant C57 mice at day 11.5 of gestation after treating with 100nM
562 BMS-754809 (HY10200; MedChemExpress; USA) or PBS for three days in vitro.

563 **Mass cytometry by time of flight**

564 Placental villi rather than chorionic plate and extraplacental membranes were used for
565 CyToF in this study. 8 × 10^5 immune cells from NP (n=9), PE (n=8), GDM (n=8), GDM&PE
566 (n=7) presented in Table 1 were washed once with 1x PBS and then stained with 100μL of 2.5
567 μM cisplatin (Fluidigm) for 5min on ice to exclude dead cells, and then incubated in Fc receptor

568 blocking solution before stained with surface antibodies cocktail for 30 min on ice. Cells were
569 washed twice with FACS buffer (1xPBS+0.5%BSA) and fixed in 200μL of intercalation solution
570 (Maxpar Fix and Perm Buffer containing 250nM 191/193Ir, Fluidigm) overnight. After fixation,
571 cells were washed once with FACS buffer and then perm buffer (eBioscience), stained with
572 intracellular antibodies cocktail for 30 min on ice. Cells were washed and resuspend with
573 deionized water, adding into 20% EQ beads (Fluidigm), acquired on a mass cytometer (Helios,
574 Fluidigm). Additionally, all PE samples enumerated in Table 1 demonstrate a late-onset
575 preeclampsia, with placental specimens being procured from patients more than 35 weeks of
576 gestation and less than the 38 weeks of pregnancy.
577 As for data analysis, data of each sample were debarcoded from raw data using a
578 doublet-filtering scheme with unique mass-tagged barcodes firstly. Each .fcs file generated
579 from different batches were normalized through bead normalization method. Then we
580 manually gate data using a FlowJo software to exclude to debris, dead cells and doublets,
581 leaving live, single immune cells. Subsequently we applied the Phenograph clustering
582 algorithm to all cells to partition the cells into distinct phenotypes based on marker expression
583 levels. Cell type of each cluster according to its marker expression pattern on a heatmap of
584 cluster vs marker was annotated. Finally, we used the dimensionality reduction algorithm
585 t-SNE to visualize the high-dimensional data in two dimensions and show distribution of each
586 cluster and marker expression and difference among each group or different sample type.
587 **RNA sequencing**
588 5×10^5 $CD45^+F4/80^+CD206^-$ pro-inflam Macs (n=3) and 5×10^5 $CD45^+F4/80^+CD206^+$
589 anti-inflam Macs (n=3) were isolated from the uterus and placentas of mice with RUPP
590 and high throughput sequencing and bioinformatics analyses were conducted at Shenzhen
591 Huada Gene Technology Service Co. Ltd.(Shenzhen, China). Only differential genes with more
592 than two-fold change and a corrected P value less than 0.05 were considered statistically
593 significant.
594 **Single-cell RNA sequencing (scRNA-seq)**
595 Mice were injected with 5×10^5 $CD45^+F4/80^+CD206^-$ pro-inflam Macs or 5×10^5
596 $CD45^+F4/80^+CD206^+$ anti-inflam Macs at 12.5 days of gestation and euthanized on day 18.5 of
597 gestation. $CD45^+$ immune cells from the uterus and placenta were isolated from mice
598 transferred pro-inflam Macs and anti-inflam Macs. scRNA-seq was conducted at PLTTECH
599 Service Co. Ltd. (Hangzhou, China).
600 Firstly, the outcomes of cellular high-throughput sequencing were preserved in the FASTQ
601 file format, facilitating a rigorous evaluation of the raw data. Subsequently, the data underwent
602 debarcoding, enabling its alignment with the reference genome to precisely identify and sieve
603 effective cells. This process culminated in the construction of a comprehensive gene-barcode
604 expression matrix.For the statistical analysis and visualization of gene expression levels and
605 Unique Molecular Identifier (UMI) counts, we leveraged the powerful Seurat software.
606 Furthermore, we conducted a Clustering analysis rooted in the gene-barcode expression
607 matrix, utilizing Seurat's capabilities in conjunction with Principal Component Analysis (PCA)
608 for dimensionality reduction. This allowed us to scale down the clustering results and visually
609 represent them in two dimensions using either Uniform Manifold Approximation and Projection
610 (UMAP) or t-Distributed Stochastic Neighbor Embedding (tSNE). To gain deeper insights, we
611 performed Marker genes analysis, which hinged on the clustering outcomes. This enabled us

612 to pinpoint the genes that significantly distinguished each subgroup, thereby identifying their
613 characteristic genes. Additionally, we analyzed and graphically represented the varying
614 expression levels of these genes across different groups, providing a comprehensive
615 understanding of their differences.

616 **Isolation of NP-EVs and PE-EVs**

617 NP-EVs and PE-EVs were isolated and identified using our published protocols (Jiang et
618 al., 2021; X. Liu et al., 2022). Briefly, after digesting the placental tissues from NP or PE, the
619 suspensions were filtered through 100-μm nylon mesh and centrifugated at 3,000×g for 15
620 minutes. Then the supernatants were filtered with a 0.22-μm filter and centrifuged at
621 100,000×g for 1h at 4 °C. Then the pellets of EVs were resuspended and centrifuged at
622 100,000×g once again. A BCA assay kit conducted Protein quantitation of EVs (23235, Thermo
623 Fisher Scientific). To isolate the T-EVs, 500 μg of the EVs were incubated with 1 μg placental
624 alkaline phosphatase antibody (SC-47691, Santa Cruz Biotechnology) at 4 °C overnight, then
625 washed in the recommended buffer (PBS containing 2% exosome-free FBS and 1 mmol/L
626 ethylenediaminetetraacetic acid), and centrifuged at 100 000×g for 1 hour at 4 °C. After
627 resuspended, the total EVs were sorted by EasySep Mouse PE Positive Selection Kit II (17666,
628 STEMCELL) to collect the final NP-EVs or PE-EVs.

629 **Induction of $CD4^+$ memory-like T cells**

630 Macrophages were obtained after five days of culture of mononuclear cells isolated from
631 human peripheral blood following previous protocols (X. Liu et al., 2022). NP-EVs or PE-EVs in
632 a 50 μg/mL concentration were added to macrophages and co-cultured at 37 °C for 8 h. The
633 human $CD4^+$ naïve T cells Isolation Kit (19555, STEMCELL, Canada) was used to isolate
634 purified $CD4^+$ naïve T cells from human peripheral blood cells according to the manufacturer's
635 instructions. Then, $CD4^+$ naïve T cells were co-cultured with EV-treated macrophages for six
636 days. Flow cytometry was performed to measure the frequency of memory-like Th17 cells. For
637 animal experiments, $CD4^+$ naïve T cells sorted from the uterus and placentas of pregnant mice
638 were cultured with the IGF1R inhibitor BMS-754807 at a concentration of 10 μM for three days
639 before co-cultured with macrophages.

640 **Flow cytometry**

641 Single immune cells from the mice uterus were obtained following the method described
642 above. After incubation with Cell Stimulation Cocktail (00-4975-93, Invitrogen, USA) for five
643 hours at 37 °C, cells were collected and surface staining for either phycoerythrin-conjugated
644 anti-mouse CD4 (12-0041-82, eBioscience, USA), APC-conjugated anti-mouse CD8 (100711,
645 BioLegend, USA), phycoerythrin-Cy5.5-conjugated anti-mouse CD44 (45-0441-82,
646 eBioscience, USA), APC-conjugated anti-mouse CD11b (101212, BioLegend, USA),
647 FITC-conjugated anti-mouse Gr-1 (108406, BioLegend, USA), PE-Cyanine7-conjugated
648 anti-mouse Ly6G (E-AB-F1108H, elabscience, China) or intracellular staining for
649 488-conjugated anti-mouse IL-17A (506910, BioLegend, USA) was performed according to the
650 manufacturer's instructions.

651 Single placental and peripheral lymphocytes and were obtained following the method
652 described above. The Human Central and Effector Memory $CD4^+$ T cell Isolation Kit (17865,
653 STEMCELL, Canada) was used to obtain purified memory $CD4^+$ T cells, according to the
654 manufacturer's instructions. After incubation with Cell Stimulation Cocktail (00-4975-93,
655 Invitrogen, USA) for five hours at 37 °C, cells were collected and surface staining for

phycoerythrin-conjugated anti-human CD4 (2384240, eBioscience, USA), FITC-conjugated anti-human CD45RO (304204, BioLegend, USA), and phycoerythrin-Cy7-conjugated anti-human CCR7 (353227, BioLegend, USA) or intracellular staining for APC-conjugated anti-human IL-17A (17-7179-42, eBioscience, USA) and Foxp3 (320014, BioLegend, USA) was performed according to the manufacturer's instructions.

Immunofluorescence

Frozen sections of the placentas were permeabilized with PBS containing 0.5% Triton X-100 (PBST) for 20 min and incubated for 1 h with a blocking buffer in PBST. The sections were then incubated with anti-CD4 (sc-1176, Santa Cruz Biotechnology, China) and FITC-conjugated anti-human CD45RO (304204, BioLegend, USA) at 4 °C overnight, followed by Alexa Fluor 568-conjugated secondary antibodies (dilution: 1:200, Yeasen, China) for 1 h. The slides were counterstained with 4,6-diamidino-2-phenylindole (DAPI, 1 μg/ml; Roche, Switzerland) for 20 min. Digital images were obtained using confocal fluorescence microscopy (ZEISS LSM 800, Germany). ImageJ software was used to quantify the fluorescence intensity from immunofluorescence (IF) images.

Statistical analysis

Data were analyzed using SPSS version 20. After the Shapiro-wilk test, the data were confirmed to be non-normal distribution. Kruskal-wallis test was used to compare the results of experiments with multiple groups. Student's t-test was used to compare the results of experiments with two groups. All data are presented as mean ± SEM (*$P < 0.05$, ** $P < 0.01$, *** $P < 0.001$; NS, not significant).

Acknowledgments

The authors would like to express their heartfelt gratitude to the participants for their contributions. This work was financially supported by the National Natural Science Foundation of China (82271694, 82061160494), the "Pioneer" and "Leading Goose" R&D Program of Zhejiang (2023C03033), the Zhejiang Province Natural Science Foundation key project fund (LZ24H040002), the Zhejiang Medicine and Health Science and Technology Plan Project (2023KY800).

References

Agbaglo, E., Agbadi, P., Tetteh, J. K., Ameyaw, E. K., Adu, C., & Nutor, J. J. 2022. Trends in total fertility rate in Ghana by different inequality dimensions from 1993 to 2014. *BMC Womens Health* **22**: 49. DOI: https://doi.org/10.1186/s12905-022-01629-w, PMID: 35197037

Amador, C. A., Barrientos, V., Peña, J., Herrada, A. A., González, M., Valdés, S., Carrasco, L., Alzamora, R., Figueroa, F., Kalergis, A. M., & Michea, L. 2014. Spironolactone decreases DOCA-salt-induced organ damage by blocking the activation of T helper 17 and the downregulation of regulatory T lymphocytes. *Hypertension* **63**: 797-803. DOI: https://doi.org/10.1161/hypertensionaha.113.02883, PMID: 24420551

Aneman, I., Pienaar, D., Suvakov, S., Simic, T. P., Garovic, V. D., & McClements, L. 2020. Mechanisms of Key Innate Immune Cells in Early- and Late-Onset Preeclampsia. *Front Immunol* **11**: 1864. DOI: https://doi.org/10.3389/fimmu.2020.01864, PMID: 33013837

Bachmayer, N., Rafik Hamad, R., Liszka, L., Bremme, K., & Sverremark-Ekström, E. 2006. Aberrant uterine natural killer (NK)-cell expression and altered placental and serum levels

700 of the NK-cell promoting cytokine interleukin-12 in pre-eclampsia. *Am J Reprod Immunol*
701 **56**: 292-301. DOI: https://doi.org/10.1111/j.1600-0897.2006.00429.x, PMID: 17076673
702 Bekkering, S., Arts, R. J. W., Novakovic, B., Kourtzelis, I., van der Heijden, C., Li, Y., Popa, C.
703 D., Ter Horst, R., van Tuijl, J., Netea-Maier, R. T., van de Veerdonk, F. L., Chavakis, T.,
704 Joosten, L. A. B., van der Meer, J. W. M., Stunnenberg, H., Riksen, N. P., & Netea, M. G.
705 2018. Metabolic Induction of Trained Immunity through the Mevalonate Pathway. *Cell*
706 **172**: 135-146.e139. DOI: https://doi.org/10.1016/j.cell.2017.11.025, PMID: 29328908
707 Bernardes, T. P., Mol, B. W., Ravelli, A. C. J., van den Berg, P. P., Boezen, H. M., & Groen, H.
708 2019. Recurrence risk of preeclampsia in a linked population-based cohort: Effects of first
709 pregnancy maximum diastolic blood pressure and gestational age. *Pregnancy Hypertens*
710 **15**: 32-36. DOI: https://doi.org/10.1016/j.preghy.2018.10.010, PMID: 30825924
711 Burton, G. J., Redman, C. W., Roberts, J. M., & Moffett, A. 2019. Pre-eclampsia:
712 pathophysiology and clinical implications. *Bmj* **366**: l2381. DOI:
713 https://doi.org/10.1136/bmj.l2381, PMID: 31307997
714 Care, A. S., Bourque, S. L., Morton, J. S., Hjartarson, E. P., Robertson, S. A., & Davidge, S. T.
715 2018. Reduction in Regulatory T Cells in Early Pregnancy Causes Uterine Artery
716 Dysfunction in Mice. *Hypertension* **72**: 177-187. DOI:
717 https://doi.org/10.1161/hypertensionaha.118.10858, PMID: 29785960
718 Chappell, L. C., Cluver, C. A., Kingdom, J., & Tong, S. 2021. Pre-eclampsia. *Lancet* **398**:
719 341-354. DOI: https://doi.org/10.1016/s0140-6736(20)32335-7, PMID: 34051884
720 Chatterjee, P., Chiasson, V. L., Seerangan, G., De Guzman, E., Milad, M., Bounds, K. R.,
721 Gasheva, O., Tobin, R. P., Hatahet, M., Kopriva, S., Jones, K. A., Newell-Rogers, M. K., &
722 Mitchell, B. M. 2017. Depletion of MHC class II invariant chain peptide or γ-δ T-cells
723 ameliorates experimental preeclampsia. *Clin Sci (Lond)* **131**: 2047-2058. DOI:
724 https://doi.org/10.1042/cs20171008, PMID: 28642294
725 Chen, B., Ye, B., Li, M., Wang, S., Li, J., Lai, Y., Yang, N., Ke, Z., & Zhang, H. 2022. TIGIT
726 Deficiency Protects Mice From DSS-Induced Colitis by Regulating IL-17A-Producing
727 CD4(+) Tissue-Resident Memory T Cells. *Front Immunol* **13**: 931761. DOI:
728 https://doi.org/10.3389/fimmu.2022.931761, PMID: 35844584
729 Cornelius, D. C., Amaral, L. M., Harmon, A., Wallace, K., Thomas, A. J., Campbell, N., Scott, J.,
730 Herse, F., Haase, N., Moseley, J., Wallukat, G., Dechend, R., & LaMarca, B. 2015a. An
731 increased population of regulatory T cells improves the pathophysiology of placental
732 ischemia in a rat model of preeclampsia. *Am J Physiol Regul Integr Comp Physiol* **309**:
733 R884-891. DOI: https://doi.org/10.1152/ajpregu.00154.2015, PMID: 26290102
734 Cornelius, D. C., Castillo, J., Porter, J., Amaral, L. M., Campbell, N., Paige, A., Thomas, A. J.,
735 Harmon, A., Cunningham, M. W., Jr., Wallace, K., Herse, F., Wallukat, G., Dechend, R., &
736 LaMarca, B. 2015b. Blockade of CD40 ligand for intercellular communication reduces
737 hypertension, placental oxidative stress, and AT1-AA in response to adoptive transfer of
738 CD4+ T lymphocytes from RUPP rats. *Am J Physiol Regul Integr Comp Physiol* **309**:
739 R1243-1250. DOI: https://doi.org/10.1152/ajpregu.00273.2015, PMID: 26310940
740 Corrêa-Silva, S., Alencar, A. P., Moreli, J. B., Borbely, A. U., de, S. L. L., Scavone, C.,
741 Damasceno, D. C., Rudge, M. V. C., Bevilacqua, E., & Calderon, I. M. P. 2018.
742 Hyperglycemia induces inflammatory mediators in the human chorionic villous. *Cytokine*
743 **111**: 41-48. DOI: https://doi.org/10.1016/j.cyto.2018.07.020, PMID: 30114628

744 Deer, E., Herrock, O., Campbell, N., Cornelius, D., Fitzgerald, S., Amaral, L. M., & LaMarca, B.
745 2023. The role of immune cells and mediators in preeclampsia. *Nat Rev Nephrol* **19**:
746 257-270. DOI: https://doi.org/10.1038/s41581-022-00670-0, PMID: 36635411
747 Deer, E., Reeve, K. E., Amaral, L., Vaka, V. R., Franks, M., Campbell, N., Fitzgerald, S.,
748 Herrock, O., Ibrahim, T., Cornelius, D., & LaMarca, B. 2021. CD4+ T cells cause renal and
749 placental mitochondrial oxidative stress as mechanisms of hypertension in response to
750 placental ischemia. *Am J Physiol Renal Physiol* **320**: F47-f54. DOI:
751 https://doi.org/10.1152/ajprenal.00398.2020, PMID: 33196321
752 Díaz, E., Cárdenas, M., Ariza, A. C., Larrea, F., & Halhali, A. 2005. Placental insulin and
753 insulin-like growth factor I receptors in normal and preeclamptic pregnancies. *Clin*
754 *Biochem* **38**: 243-247. DOI: https://doi.org/10.1016/j.clinbiochem.2004.10.013, PMID:
755 15708546
756 DiToro, D., Harbour, S. N., Bando, J. K., Benavides, G., Witte, S., Laufer, V. A., Moseley, C.,
757 Singer, J. R., Frey, B., Turner, H., Bruning, J., Darley-Usmar, V., Gao, M., Conover, C.,
758 Hatton, R. D., Frank, S., Colonna, M., & Weaver, C. T. 2020. Insulin-Like Growth Factors
759 Are Key Regulators of T Helper 17 Regulatory T Cell Balance in Autoimmunity. *Immunity*
760 **52**: 650-667.e610. DOI: https://doi.org/10.1016/j.immuni.2020.03.013, PMID: 32294406
761 Eghbal-Fard, S., Yousefi, M., Heydarlou, H., Ahmadi, M., Taghavi, S., Movasaghpour, A.,
762 Jadidi-Niaragh, F., Yousefi, B., Dolati, S., Hojjat-Farsangi, M., Rikhtegar, R., Nouri, M., &
763 Aghebati-Maleki, L. 2019. The imbalance of Th17/Treg axis involved in the pathogenesis
764 of preeclampsia. *J Cell Physiol* **234**: 5106-5116. DOI: https://doi.org/10.1002/jcp.27315,
765 PMID: 30277561
766 Faas, M. M., Spaans, F., & De Vos, P. 2014. Monocytes and macrophages in pregnancy and
767 pre-eclampsia. *Front Immunol* **5**: 298. DOI: https://doi.org/10.3389/fimmu.2014.00298,
768 PMID: 25071761
769 Fanelli, G., Romano, M., Nova-Lamperti, E., Werner Sunderland, M., Nerviani, A., Scottà, C.,
770 Bombardieri, M., Quezada, S. A., Sacks, S. H., Noelle, R. J., Pitzalis, C., Lechler, R. I.,
771 Lombardi, G., & Becker, P. D. 2021. PD-L1 signaling on human memory CD4+ T cells
772 induces a regulatory phenotype. *PLoS Biol* **19**: e3001199. DOI:
773 https://doi.org/10.1371/journal.pbio.3001199, PMID: 33901179
774 Fu, B., Li, X., Sun, R., Tong, X., Ling, B., Tian, Z., & Wei, H. 2013. Natural killer cells promote
775 immune tolerance by regulating inflammatory TH17 cells at the human maternal-fetal
776 interface. *Proc Natl Acad Sci U S A* **110**: E231-240. DOI:
777 https://doi.org/10.1073/pnas.1206322110, PMID: 23271808
778 Fu, B., Tian, Z., & Wei, H. 2014. TH17 cells in human recurrent pregnancy loss and
779 pre-eclampsia. *Cell Mol Immunol* **11**: 564-570. DOI: https://doi.org/10.1038/cmi.2014.54,
780 PMID: 25027967
781 Fukui, A., Funamizu, A., Yokota, M., Yamada, K., Nakamua, R., Fukuhara, R., Kimura, H., &
782 Mizunuma, H. 2011. Uterine and circulating natural killer cells and their roles in women
783 with recurrent pregnancy loss, implantation failure and preeclampsia. *J Reprod Immunol*
784 **90**: 105-110. DOI: https://doi.org/10.1016/j.jri.2011.04.006, PMID: 21632120
785 Grotegut, C. A. 2016. Prevention of preeclampsia. *J Clin Invest* **126**: 4396-4398. DOI:
786 https://doi.org/10.1172/jci91300, PMID: 27841760
787 Han, X., Li, W., Li, P., Zheng, Z., Lin, B., Zhou, B., Guo, K., He, P., & Yang, J. 2021. Stimulation

788 of α7 Nicotinic Acetylcholine Receptor by Nicotine Suppresses Decidual M1 Macrophage
789 Polarization Against Inflammation in Lipopolysaccharide-Induced Preeclampsia-Like
790 Mouse Model. *Front Immunol* **12**: 642071. DOI:
791 https://doi.org/10.3389/fimmu.2021.642071, PMID: 33995360
792 Jensen, F., Wallukat, G., Herse, F., Budner, O., El-Mousleh, T., Costa, S. D., Dechend, R., &
793 Zenclussen, A. C. 2012. CD19+CD5+ cells as indicators of preeclampsia. *Hypertension*
794 **59**: 861-868. DOI: https://doi.org/10.1161/hypertensionaha.111.188276, PMID: 22353610
795 Jiang, L., Fei, H., Jin, X., Liu, X., Yang, C., Li, C., Chen, J., Yang, A., Zhu, J., Wang, H., Fei, X.,
796 & Zhang, S. 2021. Extracellular Vesicle-Mediated Secretion of HLA-E by Trophoblasts
797 Maintains Pregnancy by Regulating the Metabolism of Decidual NK Cells. *Int J Biol Sci*
798 **17**: 4377-4395. DOI: https://doi.org/10.7150/ijbs.63390, PMID: 34803505
799 Jung, E., Romero, R., Yeo, L., Gomez-Lopez, N., Chaemsaithong, P., Jaovisidha, A., Gotsch,
800 F., & Erez, O. 2022. The etiology of preeclampsia. *Am J Obstet Gynecol* **226**: S844-s866.
801 DOI: https://doi.org/10.1016/j.ajog.2021.11.1356, PMID: 35177222
802 Kieffer, T. E. C., Laskewitz, A., Scherjon, S. A., Faas, M. M., & Prins, J. R. 2019. Memory T
803 Cells in Pregnancy. *Front Immunol* **10**: 625. DOI:
804 https://doi.org/10.3389/fimmu.2019.00625, PMID: 31001255
805 Köstlin-Gille, N., Dietz, S., Schwarz, J., Spring, B., Pauluschke-Fröhlich, J., Poets, C. F., &
806 Gille, C. 2019. HIF-1α-Deficiency in Myeloid Cells Leads to a Disturbed Accumulation of
807 Myeloid Derived Suppressor Cells (MDSC) During Pregnancy and to an Increased
808 Abortion Rate in Mice. *Front Immunol* **10**: 161. DOI:
809 https://doi.org/10.3389/fimmu.2019.00161, PMID: 30804946
810 Lager, S., Sovio, U., Eddershaw, E., van der Linden, M. W., Yazar, C., Cook, E., Happerfield, L.,
811 Jessop, F. A., Sebire, N. J., Charnock-Jones, D. S., & Smith, G. C. S. 2020. Abnormal
812 placental CD8(+) T-cell infiltration is a feature of fetal growth restriction and pre-eclampsia.
813 *J Physiol* **598**: 5555-5571. DOI: https://doi.org/10.1113/jp279532, PMID: 32886802
814 LaMarca, B., Wallace, K., Herse, F., Wallukat, G., Martin, J. N., Jr., Weimer, A., & Dechend, R.
815 2011. Hypertension in response to placental ischemia during pregnancy: role of B
816 lymphocytes. *Hypertension* **57**: 865-871. DOI:
817 https://doi.org/10.1161/hypertensionaha.110.167569, PMID: 21357287
818 Lampé, R., Kövér, Á., Szűcs, S., Pál, L., Árnyas, E., Ádány, R., & Póka, R. 2015. Phagocytic
819 index of neutrophil granulocytes and monocytes in healthy and preeclamptic pregnancy. *J*
820 *Reprod Immunol* **107**: 26-30. DOI: https://doi.org/10.1016/j.jri.2014.11.001, PMID:
821 25534923
822 Lampé, R., Szucs, S., Adány, R., & Póka, R. 2011. Granulocyte superoxide anion production
823 and regulation by plasma factors in normal and preeclamptic pregnancy. *J Reprod*
824 *Immunol* **89**: 199-206. DOI: https://doi.org/10.1016/j.jri.2011.01.019, PMID: 21529965
825 Lang, X., Liu, W., Hou, Y., Zhao, W., Yang, X., Chen, L., Yan, Q., & Cheng, W. 2021. IL-17A
826 polymorphism (rs2275913) and levels are associated with preeclampsia pathogenesis in
827 Chinese patients. *BMC Med Genomics* **14**: 5. DOI:
828 https://doi.org/10.1186/s12920-020-00840-8, PMID: 33407460
829 Lewis, E. L., Sierra, L. J., Barila, G. O., Brown, A. G., Porrett, P. M., & Elovitz, M. A. 2018.
830 Placental immune state shifts with gestational age. *Am J Reprod Immunol* **79**: e12848.
831 DOI: https://doi.org/10.1111/aji.12848, PMID: 29577513

832 Li, M., Sun, F., Xu, Y., Chen, L., Chen, C., Cui, L., Qian, J., Li, D., Wang, S., & Du, M. 2022.
833 Tim-3(+) decidual Mφs induced Th2 and Treg bias in decidual CD4(+)T cells and
834 promoted pregnancy maintenance via CD132. *Cell Death Dis* **13**: 454. DOI:
835 https://doi.org/10.1038/s41419-022-04899-2, PMID: 35550500
836 Liao, G., Cheng, D., Li, J., & Hu, S. 2021. Clinical significance of microRNA-320a and
837 insulin-like growth factor-1 receptor in early-onset preeclampsia patients. *Eur J Obstet*
838 *Gynecol Reprod Biol* **263**: 164-170. DOI: https://doi.org/10.1016/j.ejogrb.2021.06.032,
839 PMID: 34218203
840 Lisonkova, S., & Joseph, K. S. 2013. Incidence of preeclampsia: risk factors and outcomes
841 associated with early- versus late-onset disease. *Am J Obstet Gynecol* **209**:
842 544.e541-544.e512. DOI: https://doi.org/10.1016/j.ajog.2013.08.019, PMID: 23973398
843 Liu, D., Li, Q., Ding, H., Zhao, G., Wang, Z., Cao, C., Dai, Y., Zheng, M., Zhu, X., Wu, Q., Wang,
844 Y., Duan, H., Tang, H., Lu, X., Hou, Y., & Hu, Y. 2021. Placenta-derived IL-32β activates
845 neutrophils to promote preeclampsia development. *Cell Mol Immunol* **18**: 979-991. DOI:
846 https://doi.org/10.1038/s41423-021-00636-5, PMID: 33707686
847 Liu, X., Fei, H., Yang, C., Wang, J., Zhu, X., Yang, A., Shi, Z., Jin, X., Yang, F., Wu, D., Jiang, L.,
848 & Zhang, S. 2022. Trophoblast-Derived Extracellular Vesicles Promote Preeclampsia by
849 Regulating Macrophage Polarization. *Hypertension* **79**: 2274-2287. DOI:
850 https://doi.org/10.1161/hypertensionaha.122.19244, PMID: 35993233
851 Lu, D., Peng, Q., Chen, D., Chen, X., & Jiang, M. 2020. Expression imbalance of IL-17/IL-35 in
852 peripheral blood and placental tissue of pregnant women in preeclampsia. *Taiwan J*
853 *Obstet Gynecol* **59**: 409-414. DOI: https://doi.org/10.1016/j.tjog.2020.03.013, PMID:
854 32416889
855 Madhur, M. S., Elijovich, F., Alexander, M. R., Pitzer, A., Ishimwe, J., Van Beusecum, J. P.,
856 Patrick, D. M., Smart, C. D., Kleyman, T. R., Kingery, J., Peck, R. N., Laffer, C. L., & Kirabo,
857 A. 2021. Hypertension: Do Inflammation and Immunity Hold the Key to Solving this
858 Epidemic? *Circ Res* **128**: 908-933. DOI: https://doi.org/10.1161/circresaha.121.318052,
859 PMID: 33793336
860 McElwain, C. J., McCarthy, F. P., & McCarthy, C. M. 2021. Gestational Diabetes Mellitus and
861 Maternal Immune Dysregulation: What We Know So Far. *Int J Mol Sci* **22**. DOI:
862 https://doi.org/10.3390/ijms22084261, PMID: 33923959
863 McIntyre, H. D., Catalano, P., Zhang, C., Desoye, G., Mathiesen, E. R., & Damm, P. 2019.
864 Gestational diabetes mellitus. *Nat Rev Dis Primers* **5**: 47. DOI:
865 https://doi.org/10.1038/s41572-019-0098-8, PMID: 31296866
866 Miller, D., Garcia-Flores, V., Romero, R., Galaz, J., Pique-Regi, R., & Gomez-Lopez, N. 2022.
867 Single-Cell Immunobiology of the Maternal-Fetal Interface. *J Immunol* **209**: 1450-1464.
868 DOI: https://doi.org/10.4049/jimmunol.2200433, PMID: 36192116
869 Morita, K., Tsuda, S., Kobayashi, E., Hamana, H., Tsuda, K., Shima, T., Nakashima, A.,
870 Ushijima, A., Kishi, H., & Saito, S. 2020. Analysis of TCR Repertoire and PD-1 Expression
871 in Decidual and Peripheral CD8(+) T Cells Reveals Distinct Immune Mechanisms in
872 Miscarriage and Preeclampsia. *Front Immunol* **11**: 1082. DOI:
873 https://doi.org/10.3389/fimmu.2020.01082, PMID: 32582176
874 Nerenberg, K. A., Johnson, J. A., Leung, B., Savu, A., Ryan, E. A., Chik, C. L., & Kaul, P. 2013.
875 Risks of gestational diabetes and preeclampsia over the last decade in a cohort of Alberta

876 women. *J Obstet Gynaecol Can* **35**: 986-994. DOI:
877 https://doi.org/10.1016/s1701-2163(15)30786-6, PMID: 24246398
878 Novotny, S. R., Wallace, K., Heath, J., Moseley, J., Dhillon, P., Weimer, A., Wallukat, G., Herse,
879 F., Wenzel, K., Martin, J. N., Jr., Dechend, R., & Lamarca, B. 2012. Activating
880 autoantibodies to the angiotensin II type I receptor play an important role in mediating
881 hypertension in response to adoptive transfer of CD4+ T lymphocytes from placental
882 ischemic rats. *Am J Physiol Regul Integr Comp Physiol* **302**: R1197-1201. DOI:
883 https://doi.org/10.1152/ajpregu.00623.2011, PMID: 22461177
884 Ostlund, I., Haglund, B., & Hanson, U. 2004. Gestational diabetes and preeclampsia. *Eur J*
885 *Obstet Gynecol Reprod Biol* **113**: 12-16. DOI:
886 https://doi.org/10.1016/j.ejogrb.2003.07.001, PMID: 15036703
887 Rasmussen, T. A., Zerbato, J. M., Rhodes, A., Tumpach, C., Dantanarayana, A., McMahon, J.
888 H., Lau, J. S. Y., Chang, J. J., Gubser, C., Brown, W., Hoh, R., Krone, M., Pascoe, R.,
889 Chiu, C. Y., Bramhall, M., Lee, H. J., Haque, A., Fromentin, R., Chomont, N., Milush, J., et
890 al. 2022. Memory CD4(+) T cells that co-express PD1 and CTLA4 have reduced response
891 to activating stimuli facilitating HIV latency. *Cell Rep Med* **3**: 100766. DOI:
892 https://doi.org/10.1016/j.xcrm.2022.100766, PMID: 36198308
893 Robajac, D., Masnikosa, R., Miković, Ž., Mandić, V., & Nedić, O. 2015. Oxidation of placental
894 insulin and insulin-like growth factor receptors in mothers with diabetes mellitus or
895 preeclampsia complicated with intrauterine growth restriction. *Free Radic Res* **49**:
896 984-989. DOI: https://doi.org/10.3109/10715762.2015.1020798, PMID: 25812587
897 Rowe, J. H., Ertelt, J. M., Xin, L., & Way, S. S. 2012. Pregnancy imprints regulatory memory
898 that sustains anergy to fetal antigen. *Nature* **490**: 102-106. DOI:
899 https://doi.org/10.1038/nature11462, PMID: 23023128
900 Saito, S., Shiozaki, A., Nakashima, A., Sakai, M., & Sasaki, Y. 2007. The role of the immune
901 system in preeclampsia. *Mol Aspects Med* **28**: 192-209. DOI:
902 https://doi.org/10.1016/j.mam.2007.02.006, PMID: 17433431
903 Santner-Nanan, B., Peek, M. J., Khanam, R., Richarts, L., Zhu, E., Fazekas de St Groth, B., &
904 Nanan, R. 2009. Systemic increase in the ratio between Foxp3+ and IL-17-producing
905 CD4+ T cells in healthy pregnancy but not in preeclampsia. *J Immunol* **183**: 7023-7030.
906 DOI: https://doi.org/10.4049/jimmunol.0901154, PMID: 19915051
907 Sasaki, Y., Darmochwal-Kolarz, D., Suzuki, D., Sakai, M., Ito, M., Shima, T., Shiozaki, A.,
908 Rolinski, J., & Saito, S. 2007. Proportion of peripheral blood and decidual CD4(+)
909 CD25(bright) regulatory T cells in pre-eclampsia. *Clin Exp Immunol* **149**: 139-145. DOI:
910 https://doi.org/10.1111/j.1365-2249.2007.03397.x, PMID: 17459078
911 Schneider, S., Freerksen, N., Röhrig, S., Hoeft, B., & Maul, H. 2012. Gestational diabetes and
912 preeclampsia--similar risk factor profiles? *Early Hum Dev* **88**: 179-184. DOI:
913 https://doi.org/10.1016/j.earlhumdev.2011.08.004, PMID: 21890288
914 Schonkeren, D., van der Hoorn, M. L., Khedoe, P., Swings, G., van Beelen, E., Claas, F., van
915 Kooten, C., de Heer, E., & Scherjon, S. 2011. Differential distribution and phenotype of
916 decidual macrophages in preeclamptic versus control pregnancies. *Am J Pathol* **178**:
917 709-717. DOI: https://doi.org/10.1016/j.ajpath.2010.10.011, PMID: 21281803
918 Shields, C. A., McCalmon, M., Ibrahim, T., White, D. L., Williams, J. M., LaMarca, B., &
919 Cornelius, D. C. 2018. Placental ischemia-stimulated T-helper 17 cells induce

920 preeclampsia-associated cytolytic natural killer cells during pregnancy. *Am J Physiol*
921 *Regul Integr Comp Physiol* **315**: R336-r343. DOI:
922 https://doi.org/10.1152/ajpregu.00061.2018, PMID: 29718698
923 Spradley, F. T., Palei, A. C., & Granger, J. P. 2015. Immune Mechanisms Linking Obesity and
924 Preeclampsia. *Biomolecules* **5**: 3142-3176. DOI: https://doi.org/10.3390/biom5043142,
925 PMID: 26569331
926 Travis, O. K., White, D., Baik, C., Giachelli, C., Thompson, W., Stubbs, C., Greer, M., Lemon, J.
927 P., Williams, J. M., & Cornelius, D. C. 2020. Interleukin-17 signaling mediates cytolytic
928 natural killer cell activation in response to placental ischemia. *Am J Physiol Regul Integr*
929 *Comp Physiol* **318**: R1036-r1046. DOI: https://doi.org/10.1152/ajpregu.00285.2019,
930 PMID: 32320265
931 Wallace, K., Novotny, S., Heath, J., Moseley, J., Martin, J. N., Jr., Owens, M. Y., & LaMarca, B.
932 2012. Hypertension in response to CD4(+) T cells from reduced uterine perfusion
933 pregnant rats is associated with activation of the endothelin-1 system. *Am J Physiol Regul*
934 *Integr Comp Physiol* **303**: R144-149. DOI: https://doi.org/10.1152/ajpregu.00049.2012,
935 PMID: 22647295
936 Wang, S., Zhu, X., Xu, Y., Zhang, D., Li, Y., Tao, Y., Piao, H., Li, D., & Du, M. 2016.
937 Programmed cell death-1 (PD-1) and T-cell immunoglobulin mucin-3 (Tim-3) regulate
938 CD4+ T cells to induce Type 2 helper T cell (Th2) bias at the maternal-fetal interface. *Hum*
939 *Reprod* **31**: 700-711. DOI: https://doi.org/10.1093/humrep/dew019, PMID: 26908841
940 Weissgerber, T. L., & Mudd, L. M. 2015. Preeclampsia and diabetes. *Curr Diab Rep* **15**: 9.
941 DOI: https://doi.org/10.1007/s11892-015-0579-4, PMID: 25644816
942 Yao, Y., Xu, X. H., & Jin, L. 2019. Macrophage Polarization in Physiological and Pathological
943 Pregnancy. *Front Immunol* **10**: 792. DOI: https://doi.org/10.3389/fimmu.2019.00792,
944 PMID: 31037072
945 Zhong, X., Gao, W., Degauque, N., Bai, C., Lu, Y., Kenny, J., Oukka, M., Strom, T. B., &
946 Rothstein, T. L. 2007. Reciprocal generation of Th1/Th17 and T(reg) cells by B1 and B2 B
947 cells. *Eur J Immunol* **37**: 2400-2404. DOI: https://doi.org/10.1002/eji.200737296, PMID:
948 17683116
949 Zhou, J., Nefedova, Y., Lei, A., & Gabrilovich, D. 2018. Neutrophils and PMN-MDSC: Their
950 biological role and interaction with stromal cells. *Semin Immunol* **35**: 19-28. DOI:
951 https://doi.org/10.1016/j.smim.2017.12.004, PMID: 29254756
952 Chen,X. , Maria ,F., Melissa,M., Jasmin,H., Igor,S., Ekaterina,A., Chanung,W., Xin,B.,
953 Mary.B.F., Hu,H., Irina,S., Kim,M.W. , Carla, M. , Jonathan,K., Maxim,N., Jason, D.,
954 David,M. 2023. Microglia-mediated T cell infiltration drives neurodegeneration in
955 tauopathy.*Nature.*615(7953):668-677.doi:10.1038/s41586-023-05788-0,PMID: 36890231.
956 Chen,J., Yang,J., Wang, W., Guo, D., Zhang, C., Wang,S., Lu, X., Huang,X., Wang,P.,
957 Zhang,G., Zhang,J., Wang,J., Cai,Z. 2022. Tumor extracellular vesicles mediate
958 anti-PD-L1 therapy resistance by decoying anti-PD-L1. Cell Mol Immunol.
959 19(11):1290-1301. doi: 10.1038/s41423-022-00926-6, PMID: 36220994.
960 Nalio Ramos R, Missolo-Koussou Y, Gerber-Ferder Y, Bromley CP, Bugatti M, Núñez NG,
961 Tosello Boari J, Richer W, Menger L, Denizeau J, Sedlik C, Caudana P, Kotsias F, Niborski
962 LL, Viel S, Bohec M, Lameiras S, Baulande S, Lesage L, Nicolas A, Meseure D,
963 Vincent-Salomon A, Reyal F, Dutertre CA, Ginhoux F, Vimeux L, Donnadieu E, Buttard B,

964 Galon J, Zelenay S, Vermi W, Guermonprez P, Piaggio E, Helft J. 2022. Tissue-resident
965 FOLR2+ macrophages associate with CD8+ T cell infiltration in human breast cancer. Cell.
966 2022 Mar 31;185(7):1189-1207.e25. doi: 10.1016/j.cell.2022.02.021, PMID: 35325594.
967 Thomas JR, Appios A, Zhao X, Dutkiewicz R, Donde M, Lee CYC, Naidu P, Lee C, Cerveira J,
968 Liu B, Ginhoux F, Burton G, Hamilton RS, Moffett A, Sharkey A, McGovern N. 2021.
969 Phenotypic and functional characterization of first-trimester human placental
970 macrophages, Hofbauer cells. J Exp Med. 2021 Jan 4;218(1):e20200891. doi:
971 10.1084/jem.20200891.PMID: 33075123.
972 Che LH, Liu JW, Huo JP, Luo R, Xu RM, He C, Li YQ, Zhou AJ, Huang P, Chen YY, Ni W, Zhou
973 YX, Liu YY, Li HY, Zhou R, Mo H, Li JM. A single-cell atlas of liver metastases of colorectal
974 cancer reveals reprogramming of the tumor microenvironment in response to preoperative
975 chemotherapy.Cell Discov. 2021 Sep 7;7(1):80. doi: 10.1038/s41421-021-00312-y. PMID:
976 34489408.
977 Desrumaux C, Lemaire-Ewing S, Ogier N, Yessoufou A, Hammann A, Sequeira-Le Grand A,
978 Deckert V, Pais de Barros JP, Le Guern N, Guy J, Khan NA, Lagrost L. Plasma
979 phospholipid transfer protein (PLTP) modulates adaptive immune functions through
980 alternation of T helper cell polarization. Cell Mol Immunol. 2016 Nov;13(6):795-804. doi:
981 10.1038/cmi.2015.75. Epub 2015 Aug 31. PMID: 26320740.
982 He J, Song Y, Li G, Xiao P, Liu Y, Xue Y, Cao Q, Tu X, Pan T, Jiang Z, Cao X, Lai L, Wang Q.
983 Fbxw7 increases CCL2/7 in CX3CR1hi macrophages to promote intestinal inflammation.
984 J Clin Invest. 2019 Jun 27;129(9):3877-3893. doi: 10.1172/JCI123374.PMID: 31246581.
985 Wu Y, Wu C, Shi T, Cai Q, Wang T, Xiong Y, Zhang Y, Jiang W, Lu M, Chen Z, Chen J, Wang J,
986 He R. FAP expression in adipose tissue macrophages promotes obesity and metabolic
987 inflammation. Proc Natl Acad Sci U S A. 2023 Dec 19;120(51):e2303075120. doi:
988 10.1073/pnas.2303075120. Epub 2023 Dec 15. PMID: 38100414.
989 Jin G, Guo N, Liu Y, Zhang L, Chen L, Dong T, Liu W, Zhang X, Jiang Y, Lv G, Zhao F, Liu W,
990 Hei Z, Yang Y, Ou J. 5-aminolevulinate and CHIL3/CHI3L1 treatment amid ischemia aids
991 liver metabolism and reduces ischemia-reperfusion injury. Theranostics. 2023 Aug
992 28;13(14):4802-4820. doi: 10.7150/thno.83163. eCollection 2023. PMID: 37771779.
993 Nugteren S, Samsom JN. Secretory Leukocyte Protease Inhibitor (SLPI) in mucosal tissues:
994 Protects against inflammation, but promotes cancer. Cytokine Growth Factor Rev. 2021
995 Jun;59:22-35. doi: 10.1016/j.cytogfr.2021.01.005. Epub 2021 Feb 10. PMID: 33602652.
996 Li R, Ferdinand JR, Loudon KW, Bowyer GS, Laidlaw S, Muyas F, Mamanova L, Neves JB,
997 Bolt L, Fasouli ES, Lawson ARJ, Young MD, Hooks Y, Oliver TRW, Butler TM, Armitage
998 JN, Aho T, Riddick ACP, Gnanapragasam V, Welsh SJ, Meyer KB, Warren AY, Tran MGB,
999 Stewart GD, Cortés-Ciriano I, Behjati S, Clatworthy MR, Campbell PJ, Teichmann SA,
1000 Mitchell TJ. Mapping single-cell transcriptomes in the intra-tumoral and associated
1001 territories of kidney cancer. Cancer Cell. 2022 Dec 12;40(12):1583-1599.e10. doi:
1002 10.1016/j.ccell.2022.11.001. Epub 2022 Nov 23.PMID: 36423636.
1003 Che LH, Liu JW, Huo JP, Luo R, Xu RM, He C, Li YQ, Zhou AJ, Huang P, Chen YY, Ni W,
1004 Zhou YX, Liu YY, Li HY, Zhou R, Mo H, Li JM. A single-cell atlas of liver metastases of
1005 colorectal cancer reveals reprogramming of the tumor microenvironment in response to
1006 preoperative chemotherapy. Cell Discov. 2021 Sep 7;7(1):80. doi:
1007 10.1038/s41421-021-00312-y.PMID: 34489408.

1008 Coppo L, Mishra P, Siefert N, Holmgren A, Pääbo S, Zeberg H. A substitution in the
1009 glutathione reductase lowers electron leakage and inflammation in modern humans. Sci
1010 Adv. 2022 Jan 7;8(1):eabm1148. doi: 10.1126/sciadv.abm1148. Epub 2022 Jan 5. PMID:
1011 34985944.
1012 Hang S, Paik D, Yao L, Kim E, Trinath J, Lu J, Ha S, Nelson BN, Kelly SP, Wu L, Zheng Y,
1013 Longman RS, Rastinejad F, Devlin AS, Krout MR, Fischbach MA, Littman DR, Huh JR.
1014 Bile acid metabolites control TH17 and Treg cell differentiation.Nature. 2019
1015 Dec;576(7785):143-148. doi: 10.1038/s41586-019-1785-z. Epub 2019 Nov 27. PMID:
1016 31776512.
1017 Leite JA, Menezes L, Martins E, Rodrigues TS, Tavares L, Ebering A, Schelmbauer C,
1018 Martelossi Cebinelli GC, Zinina V, Golden A, Soshnikova N, Zamboni DS, Cunha FQ,
1019 Huber M, Silva JS, Waisman A, Carlos D, Saraiva Câmara NO. AIM2 promotes TH17
1020 cells differentiation by regulating RORγt transcription activity. iScience. 2023 Oct
1021 4;26(11):108134. doi: 10.1016/j.isci.2023.108134. eCollection 2023 Nov 17. PMID:
1022 37867943.
1023 Evrard M, Becht E, Fonseca R, Obers A, Park SL, Ghabdan-Zanluqui N, Schroeder J, Christo
1024 SN, Schienstock D, Lai J, Burn TN, Clatch A, House IG, Beavis P, Kallies A, Ginhoux F,
1025 Mueller SN, Gottardo R, Newell EW, Mackay LK. Single-cell protein expression profiling
1026 resolves circulating and resident memory T cell diversity across tissues and infection
1027 contexts. Immunity. 2023 Jul 11;56(7):1664-1680.e9. doi: 10.1016/j.immuni.2023.06.005.
1028 Epub 2023 Jun 30. PMID: 37392736.
1029 Bieberich F, Vazquez-Lombardi R, Yermanos A, Ehling RA, Mason DM, Wagner B,
1030 Kapetanovic E, Di Roberto RB, Weber CR, Savic M, Rudolf F, Reddy ST. A Single-Cell
1031 Atlas of Lymphocyte Adaptive Immune Repertoires and Transcriptomes Reveals
1032 Age-Related Differences in Convalescent COVID-19 Patients. Front Immunol. 2021 Jul
1033 12;12:701085. doi: 10.3389/fimmu.2021.701085. eCollection 2021. PMID: 34322127.
1034 Qiu C, Du G. Loss of LEF-1 expression as a diagnostic indicator for extranodal NK/T-cell
1035 lymphoma: An immunohistochemical study of 88 cases. Eur J Haematol. 2022
1036 Nov;109(5):513-518. doi: 10.1111/ejh.13836. Epub 2022 Aug 2.PMID: 35871391.
1037 Sekine T, Perez-Potti A, Nguyen S, Gorin JB, Wu VH, Gostick E, Llewellyn-Lacey S, Hammer
1038 Q, Falck-Jones S, Vangeti S, Yu M, Smed-Sörensen A, Gaballa A, Uhlin M, Sandberg JK,
1039 Brander C, Nowak P, Goepfert PA, Price DA, Betts MR, Buggert M. TOX is expressed by
1040 exhausted and polyfunctional human effector memory CD8+ T cells. Sci Immunol. 2020
1041 Jul 3;5(49):eaba7918. doi: 10.1126/sciimmunol.aba7918. PMID: 32620560.
1042 Esensten JH, Helou YA, Chopra G, Weiss A, Bluestone JA. CD28 Costimulation: From
1043 Mechanism to Therapy. Immunity. 2016 May 17;44(5):973-88.
1044 doi:10.1016/j.immuni.2016.04.020. PMID: 27192564.
1045 Pai JA, Hellmann MD, Sauter JL, Mattar M, Rizvi H, Woo HJ, Shah N, Nguyen EM, Uddin FZ,
1046 Quintanal-Villalonga A, Chan JM, Manoj P, Allaj V, Baine MK, Bhanot UK, Jain M, Linkov I,
1047 Meng F, Brown D, Chaft JE, Plodkowski AJ, Gigoux M, Won HH, Sen T, Wells DK,
1048 Donoghue MTA, de Stanchina E, Wolchok JD, Loomis B, Merghoub T, Rudin CM, Chow
1049 A, Satpathy AT. Lineage tracing reveals clonal progenitors and long-term persistence of
1050 tumor-specific T cells during immune checkpoint blockade. Cancer Cell. 2023 Apr

1051 10;41(4):776-790.e7. doi: 10.1016/j.ccell.2023.03.009. Epub 2023 Mar 30. PMID:
1052 37001526.
1053 Montaldo E, Lusito E, Bianchessi V, Caronni N, Scala S, Basso-Ricci L, Cantaffa C,
1054 Masserdotti A, Barilaro M, Barresi S, Genua M, Vittoria FM, Barbiera G, Lazarevic D,
1055 Messina C, Xue E, Marktel S, Tresoldi C, Milani R, Ronchi P, Gattillo S, Santoleri L, Di
1056 Micco R, Ditadi A, Belfiori G, Aleotti F, Naldini MM, Gentner B, Gardiman E, Tamassia N,
1057 Cassatella MA, Hidalgo A, Kwok I, Ng LG, Crippa S, Falconi M, Pettinella F, Scapini P,
1058 Naldini L, Ciceri F, Aiuti A, Ostuni R. Cellular and transcriptional dynamics of human
1059 neutrophils at steady state and upon stress. Nat Immunol. 2022 Oct;23(10):1470-1483.
1060 doi: 10.1038/s41590-022-01311-1. Epub 2022 Sep 22.PMID: 36138183.
1061 Wenzel P, Rossmann H, Müller C, Kossmann S, Oelze M, Schulz A, Arnold N, Simsek C,
1062 Lagrange J, Klemz R, Schönfelder T, Brandt M, Karbach SH, Knorr M, Finger S, Neukirch
1063 C, Häuser F, Beutel ME, Kröller-Schön S, Schulz E, Schnabel RB, Lackner K, Wild PS,
1064 Zeller T, Daiber A, Blankenberg S, Münzel T. Heme oxygenase-1 suppresses a
1065 pro-inflammatory phenotype in monocytes and determines endothelial function and
1066 arterial hypertension in mice and humans. Eur Heart J. 2015 Dec 21;36(48):3437-46. doi:
1067 10.1093/eurheartj/ehv544. Epub 2015 Oct 29. PMID: 26516175.
1068 Ulff-Møller CJ, Asmar F, Liu Y, Svendsen AJ, Busato F, Grønbaek K, Tost J, Jacobsen S. Twin
1069 DNA Methylation Profiling Reveals Flare-Dependent Interferon Signature and B Cell
1070 Promoter Hypermethylation in Systemic Lupus Erythematosus. Arthritis Rheumatol. 2018
1071 Jun;70(6):878-890. doi: 10.1002/art.40422. Epub 2018 May 9. PMID: 29361205.
1072 Drummond RA, Swamydas M, Oikonomou V, Zhai B, Dambuza IM, Schaefer BC, Bohrer AC,
1073 Mayer-Barber KD, Lira SA, Iwakura Y, Filler SG, Brown GD, Hube B, Naglik JR, Hohl TM,
1074 Lionakis MS. CARD9+ microglia promote antifungal immunity via IL-1β- and
1075 CXCL1-mediated neutrophil recruitment. Nat Immunol. 2019 May;20(5):559-570. doi:
1076 10.1038/s41590-019-0377-2. Epub 2019 Apr 17. PMID: 30996332.
1077 von Wulffen M, Luehrmann V, Robeck S, Russo A, Fischer-Riepe L, van den Bosch M, van
1078 Lent P, Loser K, Gabrilovich DI, Hermann S, Roth J, Vogl T. S100A8/A9-alarmin promotes
1079 local myeloid-derived suppressor cell activation restricting severe autoimmune arthritis.
1080 Cell Rep. 2023 Aug 29;42(8):113006. doi: 10.1016/j.celrep.2023.113006. Epub 2023 Aug
1081 22. PMID: 37610870.
1082 Kao KD, Grasberger H, El-Zaatari M. The Cxcr2+ subset of the S100a8+ gastric granylocytic
1083 myeloid-derived suppressor cell population (G-MDSC) regulates gastric pathology. Front
1084 Immunol. 2023 Sep 8;14:1147695. doi: 10.3389/fimmu.2023.1147695. eCollection 2023.
1085 PMID: 37744359.
1086 Robertson SA, Green ES, Care AS, Moldenhauer LM, Prins JR, Hull ML, Barry SC, Dekker G.
1087 Therapeutic Potential of Regulatory T Cells in Preeclampsia-Opportunities and
1088 Challenges. Front Immunol. 2019 Mar 21;10:478. doi: 10.3389/fimmu.2019.00478.
1089 eCollection 2019. PMID: 30984163
1090 Sefik E, Geva-Zatorsky N, Oh S, Konnikova L, Zemmour D, McGuire AM, Burzyn D,
1091 Ortiz-Lopez A, Lobera M, Yang J, Ghosh S, Earl A, Snapper SB, Jupp R, Kasper D,
1092 Mathis D, Benoist C. MUCOSAL IMMUNOLOGY. Individual intestinal symbionts induce a
1093 distinct population of RORγ^{+} regulatory T cells. Science. 2015 Aug 28;349(6251):993-7.
1094 doi: 10.1126/science.aaa9420. Epub 2015 Aug 13. PMID: 26272906

Akkari L, Amit I, Bronte V, Fridlender ZG, Gabrilovich DI, Ginhoux F, Hedrick CC, Ostrand-Rosenberg S. Defining myeloid-derived suppressor cells. Nat Rev Immunol. 2024 Jul 5. doi: 10.1038/s41577-024-01062-0. Online ahead of print. PMID: 38969773

Aneman I, Pienaar D, Suvakov S, Simic TP, Garovic VD, McClements L.Mechanisms of Key Innate Immune Cells in Early- and Late-Onset Preeclampsia.Front Immunol. 2020 Aug 18;11:1864. doi: 10.3389/fimmu.2020.01864. eCollection 2020. PMID: 33013837

Luo F, Liu F, Guo Y, Xu W, Li Y, Yi J, Fournier T, Degrelle S, Zitouni H, Hernandez I, Liu X, Huang Y, Yue J.Single-cell profiling reveals immune disturbances landscape and HLA-F-mediated immune tolerance at the maternal-fetal interface in preeclampsia.Front Immunol. 2023 Oct 3;14:1234577. doi: 10.3389/fimmu.2023.1234577. eCollection 2023.PMID: 37854606

Li Y, Sang Y, Chang Y, Xu C, Lin Y, Zhang Y, Chiu PCN, Yeung WSB, Zhou H, Dong N, Xu L, Chen J, Zhao W, Liu L, Yu D, Zang X, Ye J, Yang J, Wu Q, Li D, Wu L, Du M. A Galectin-9-Driven CD11c^{high} Decidual Macrophage Subset Suppresses Uterine Vascular Remodeling in Preeclampsia.Circulation. 2024 May 21;149(21):1670-1688. doi:10.1161/CIRCULATIONAHA.123.064391. Epub 2024 Feb 5.PMID: 38314577

Figures with figure Legends

Figure 1 Identification and characterization of placental immune cells using CyTOF

(A) Schematic of the experimental workflow in CyTOF experiment. The placentas were obtained from individuals with normal pregnancy (NP, n=9), preeclampsia (PE, n=8), gestational diabetes mellitus (GDM, n=8) or GDM&PE (n=7).

(B) t-SNE maps showing 8×10^4 CD45$^+$ cells (the average cell number of the all samples) from the placenta overlaid with color-coded clusters and the distributions of B cells, CD4$^+$ T cells, CD8$^+$ T cells, DC, γδT cells, monocytes, granulocytes, MDSC, and NK cells.

(C) Percentages of each cell type of CD45$^+$ cells in placentas.

(D) t-SNE maps showing the expression of CD3, CD8, CD4, γδTCR, CD14, CD15, CD56.

(E) Heatmap showing the expression levels of markers in CD45$^+$ cell subsets.

Data were compared between NP and PE, NP and GDM, NP and GDM&PE using the Kruskal-wallis test and represented as mean±SEM (*P < 0.05, ** P < 0.01, *** P < 0.001; NS, not significant).

Figure 2 Specific altered T cell profile in the placentas of individuals with PE

(A) Distribution of the CD4$^+$ T cells in the group analyzed using t-SNE.

(B) Scatter dot plots showing the frequencies of cluster 8 of CD4$^+$ T cells in the placentas of individuals with NP, PE, GDM and GDM&PE (n=9 in NP group; n=8 in PE group; n=8 in GDM group; n=7 in GDM&PE group).

(C) Expression of IL-17A and Foxp3 in CD45RO$^+$CCR7$^+$CD4$^+$ T cells in placentas of individuals with NP and PE using flow cytometry (IL-17A: n=10 in NP group, n=15 in PE group; Foxp3: n=7 in NP group, n=9 in PE group).

(D) Immunofluorescence co-staining of CD4 (red), CD45RO (green) and DAPI (blue) in frozen placental sections. The right panels show the fluorescence intensity of CD4 and CD45RO.Scale bar, 20 μm.

1139 (E) Scatter dot plots showing significantly altered markers of in cluster 8 of $CD4^+$ T cells.
1140 (F) Distribution of the $CD8^+$ T cells analyzed using t-SNE.
1141 (G) Scatter dot plots showing the frequencies of cluster 2 of $CD8^+$ T cells in the placentas of
1142 individuals with NP, PE, GDM and GDM&PE.
1143 (H) Scatter dot plots showing significantly altered markers in cluster 2 of $CD8^+$ T cells.
1144 Data were compared between NP and PE, NP and GDM, NP and GDM&PE using the
1145 Kruskal-wallis test and represented as mean±SEM (*P < 0.05, ** P < 0.01, *** P < 0.001; NS,
1146 not significant).
1147 **Figure 2—figure supplement 1 Identification of the placental T cell subsets.**
1148 (A) Heatmap showing the expression levels of markers in the $CD4^+$ T subsets (n=9 in NP
1149 group; n=8 in PE group; n=8 in GDM group; n=7 in GDM&PE group).
1150 (B) Heatmap showing the expression levels of markers in the $CD8^+$ T subsets.
1151 (C) Heatmap showing the expression levels of markers in the γδT subsets.
1152 (D) Distribution of the γδT cells in the group analyzed using t-SNE.
1153 (E) Scatter dot plots showing the frequencies of cluster 15 of γδT cells in the placentas of
1154 individuals with NP, PE, GDM and GDM&PE.
1155 (F) Scatter dot plots showing significantly altered markers in cluster 15 of γδT cells.
1156 Data were compared between NP and PE, NP and GDM, NP and GDM&PE using the
1157 Kruskal-wallis test and represented as mean±SEM (*P < 0.05, ** P < 0.01, *** P < 0.001; NS,
1158 not significant).
1159
1160 **Figure 3 Identification of the placental $CD11b^+$ cell subsets and the Interaction between**
1161 **placental immune cells.**
1162 (A) Distribution of the $CD11b^+$ immune cells in group analyzed using t-SNE.
1163 (B) Heatmap showing the expression levels of markers in the $CD11b^+$ cells.
1164 (C) Scatter dot plots showing the frequencies of cluster 12, cluster 23, and cluster 25 of
1165 $CD11b^+$ cells in the placentas.
1166 (D) Interaction between placental immune cells showed in heatmap.
1167 (E) Scatter plots of Pearson's correlation analysis between placental immune cells.
1168 Data were compared between NP and PE, NP and GDM, NP and GDM&PE using the
1169 Kruskal-wallis test and represented as mean±SEM (*P < 0.05, ** P < 0.01, *** P < 0.001; NS,
1170 not significant).
1171
1172 **Figure 4 The immune imbalance at the maternal-fetal interface induced by $F480^+CD206^-$**
1173 **pro-inflam Macs.**
1174 (A) An illustration showcasing the RNA-seq of the $CD45^+F4/80^+CD206^-$ pro-inflam Macs and
1175 $CD45^+F4/80^+CD206^+$ anti-inflam Macs derived from the RUPP mouse model.
1176 (B) Principal component analysis (PCA) reflected the differences between the two groups of
1177 macrophages (n=3).
1178 (C) The volcano map shows a comparison of the content and P value of gene expression
1179 between pro-inflam Macs and anti-inflam Macs. Differential expression genes were screened
1180 out when P < 0.05. Red dots indicate genes with increased expression in pro-inflam Macs.
1181 Blue dots indicate genes with decreased expression.
1182 (D) The volcano map shows differential expression genes between pro-inflam Macs and

anti-inflam Macs.

(E) Representative pathways enriched in the identified genes as determined by GSEA (p value<0.05).

(F) Embryo abortion rate of the pregnant mice, body weight and crown-rump length of pups measured on day 18.5 of gestation. Black represents mice treated with DMSO (n=8); gray represents mice treated with PLX3397 (n=8); blue represents mice injected with $CD45^+F4/80^+CD206^+$ anti-inflammatory macrophages (n=8); red represents mice injected with $CD45^+F4/80^+CD206^-$ pro-inflammatory macrophages (n=8).

(G) SBP and UACR of pregnant mice in the four groups.

(H) Frequencies of $CD44^+CD4^+IL\text{-}17A^+$ cells, $CD44^+CD8^+$ T cells and $CD11b^+Ly6G^+$ granulocytes analyzed by flow cytometry.

Data were compared between groups using the Kruskal-wallis test and represented as mean±SEM (*P < 0.05, ** P < 0.01, *** P < 0.001).

Figure 4—figure supplement 1 The construction of RUPP mouse model

(A) Experimental design of mice model with PE by reducing uterine perfusion pressure (RUPP) on day 12.5 of gestation. Mice with sham operation were considered as controls. Systolic blood pressure (SBP) and urine albumin creatine ratio (UACR) were measured on day 12.5 and 16.5 of gestation respectively. Mice were sacrificed on day 18.5 of gestation.

(B) The embryo abortion rate of pregnant mice, body weight, and crown-rump length of pups measured on day 18.5 of gestation in the Sham and RUPP group. Embryo abortion rate = number of absorbed embryos/total number of embryos. Blue represents mice in the Sham group (n=9); Red represents mice in the RUPP group (n=9).

(C) SBP and UACR of pregnant mice in Sham and RUPP group.

(D) The embryo abortion rate of pregnant mice, body weight, and crown-rump length of pups measured on day 18.5 of gestation in the mice injected with PBS or RUPP-derived macrophages. Embryo abortion rate = number of absorbed embryos/total number of embryos. Blue represents mice in the mice injected with PBS group (n=6); Red represents mice in the mice injected with RUPP-derived macrophages group (n=6).

(E) SBP and UACR of pregnant mice in PBS and RUPP-derived macrophages group.

(F) Experimental design of GFP pregnant mice model.

(G) Frequencies of GFP^+CD11b^+ fetal-derived macrophages and GFP^-CD11b^+ maternal-derived macrophages were analyzed by flow cytometry.

Data were compared between the two groups using the Student's t-test and represented as mean±SEM (*P < 0.05, ** P < 0.01, *** P < 0.001).

Figure 4—figure supplement 2 Clodronate liposomes were used to used to deplete the macrophages of pregnant mice to demonstrate that pro-inflam Macs lead to immune imbalance.

(A) Frequencies of $F4/80^+7AAD^-$ macrophages in PLX3397-treated mouse were analyzed by flow cytometry.

(B) Frequencies of $F4/80^+7AAD^-$ macrophages in Clodronate liposomes-treated mouse were analyzed by flow cytometry.

(C) Embryo abortion rate of the pregnant mice, body weight and crown-rump length of pups measured on day 18.5 of gestation. Black represents mice treated with control liposomes (n=6); gray represents mice treated with clodronate liposomes (n=6); blue represents mice

1227 injected with $CD45^+F4/80^+CD206^+$ anti-inflam Macs (n=6); red represents mice injected with
1228 $CD45^+F4/80^+CD206^-$ pro-inflam Macs (n=6).
1229 (D) SBP and UACR of pregnant mice in the four groups.
1230 (E) Frequencies of $CD44^+CD4^+IL\text{-}17A^+$ cells, $CD44^+CD8^+$ T cells and $CD11b^+Gr1^+$
1231 granulocytes analyzed by flow cytometry.
1232 Data were compared between groups using one-way ANOVA and represented as mean±SEM
1233 (*P < 0.05, ** P < 0.01, *** P < 0.001).
1234
1235 **Figure 5 Identification of the macrophage subsets in mice injected with pro-inflam Macs**
1236 **and anti-inflam Macs by using scRNA-seq.**
1237 (A) UMAP maps showing the 8 types of mouse immune cells at the maternal-fetal interface.
1238 (B) Heatmap showing clustering analysis for markers distinguished different type of immune
1239 cells.
1240 (C) UMAP maps showing the 15 clusters of mouse macrophages was listedl.
1241 (D) Bar graph showing the frequencies of clusters of macrophages in the two groups of mice
1242 was listed in the right panel.
1243 (E) UMAP maps showing the distribution of specific markers of cluster 0 and cluster 1.
1244 (F) Dot plot depicting GO enrichment terms that were significantly enriched in the
1245 differentially expressed genes in cluster 0 and cluster 1 from the pro-inflam Macs group
1246 and the control group.
1247 (G) Violin plot of specific differential gene expression in cluster 0 and cluster 1 between the
1248 pro-inflam Macs group and the control group.
1249 Data were compared between the two groups using the Student's t-test and represented as
1250 mean±SEM (*P < 0.05, ** P < 0.01, *** P < 0.001).
1251 **Figure 5 Heatmap of different clusters of macrophages.**
1252 (A) Heatmap showing clustering analysis for markers distinguished different clusters of
1253 macrophages.
1254
1255 **Figure 6 Identification of the T/NK cells subsets in mice injected pro-inflam Macs and**
1256 **anti-inflam Macs using scRNA-seq.**
1257 (A) UMAP maps showing the 12 clusters of mouse T/NK cells was listed. Heatmap showing
1258 clustering analysis for markers distinguished 12 different clusters of T/NK cells.
1259 (B) Bar graph showing the frequencies of clusters of T/NK cells in the two groups of mice was
1260 listed in the down panel.
1261 (C) Dot plot depicting GO enrichment terms that were significantly enriched in the
1262 differentially expressed genes in cluster 0 from the pro-inflam Macs group and the control
1263 group.
1264 (D) Violin plot of specific differential gene expression in cluster 0 between the pro-inflam
1265 Macs group and the control group.
1266 (F) Frequencies of $CD4^+CD44^+$ T cells and the percentages of $Foxp3^+$ or $IL\text{-}17A^+$ cells in
1267 $CD4^+CD44^+$ T cells at the maternal-fetal interface in Sham and RUPP group analyzed by
1268 flow cytometry.
1269 (G) The embryo abortion rate of pregnant mice, body weight, and crown-rump length of pups
1270 measured on day 18.5 of gestation in mice injected PBS, Sham mouse-derived or RUPP

1271 mouse-derived $CD4^+CD44^+$ T cells. Black represents mice injected with PBS (n=6); blue
1272 represents mice injected with Sham mouse-derived $CD4^+CD44^+$ T cells (n=6); red represents
1273 mice injected with RUPP mouse-derived $CD4^+CD44^+$ T cells (n=6).
1274 (H) SBP and UACR of pregnant mice injected with PBS, Sham mouse-derived or RUPP
1275 mouse-derived $CD4^+CD44^+$ T cells.
1276 Data were compared between groups using one-way ANOVA and represented as mean±SEM
1277 (*P < 0.05, ** P < 0.01, *** P < 0.001).
1278 Data were compared between the two groups using the Student's t-test and represented as
1279 mean±SEM (*P < 0.05, ** P < 0.01, *** P < 0.001).
1280 **Figure 6—figure supplement 1 Memory-like Th17 cells may be associated with the**
1281 **recurrence of PE.**
1282 (A) Heatmap showing clustering analysis for markers distinguished 12 different clusters of
1283 T/NK cells.
1284 (B) Embryo abortion rate of pregnant mice, body weight and crown-rump length of pups
1285 measured on day 18.5 of gestation. Blue represents mice with previous normal pregnancy
1286 (n=9); red represents mice with previous pregnancy with PE (n=9).
1287 (C) SBP and UACR of second pregnant mice with a history of PE or NP in the first pregnancy
1288 measured on day 16.5 of gestation.
1289 (D) Frequencies of $CD4^+$ $CD44^+$ T cells and the levels of IL-17A in $CD4^+$ $CD44^+$ T cells in mice
1290 with a pregnancy history with NP and PE analyzed by flow cytometry.
1291 Data were compared using the Student's t-test and represented as mean±SEM (*P < 0.05, ** P
1292 < 0.01, *** P < 0.001; NS, not significant).
1293 Data were compared between the two groups using the Student's t-test and represented as
1294 mean±SEM (*P < 0.05, ** P < 0.01, *** P < 0.001).
1295 **Figure 6—figure supplement 2 Identification of the granulocytes subsets in mice**
1296 **injected pro-inflam Macs and anti-inflam Macs use sc RNA-seq.**
1297 (A) UMAP maps showing the 9 clusters of mouse granulocytes. Bar graph showing the
1298 frequencies of clusters of granulocytes in the two groups of mice.
1299 (B) Heatmap showing clustering analysis for markers distinguished 9 different clusters of
1300 granulocytes cells.
1301 (C) UMAP maps showing the distribution of specific markers of cluster 3.
1302 (D) Dot plot depicting GO enrichment terms that were significantly enriched in the
1303 differentially expressed genes in cluster 3 from the pro-inflam Macs group and the control
1304 group.
1305 (E) Violin plot of specific differential gene expression in cluster 3 between the pro-inflam
1306 Macs group and the control group.
1307 (F) Immunofluorescence co-staining of CD15 (red), CD66b (green) and DAPI (blue) in frozen
1308 placental sections. Scale bar, 20 μm.
1309 Data were compared between the two groups using the Student's t-test and represented as
1310 mean±SEM (*P < 0.05, ** P < 0.01, *** P < 0.001).
1311
1312
1313 **Figure 7 Pro-inflam Macs induce the generation of memory-like Th17 cells via**
1314 **IGF1-IGF1R**

(A) Signaling modules indicated by ligand-receptor pairing between macrophages and other types of immune cells at the maternal-fetal interface using CellPhoneDB.

(B) Frequencies of $IGF1^+CD14^+$ cells and $IGFIR^+CD4^+$ cells in placentas of individuals with NP and PE (n=12 in NP group, n=4 in PE group).

(C) Schematic of the experimental workflow to induce memory-like T cells in vitro. Macrophages, after incubating with PBS, NP-EVs or PE-EVs, were co-cultured with $CD4^+$ naïve T cells treated with DMSO or BMS-754807. Cells were isolated from human peripheral blood.

(D) Frequencies of $CD45RO^+CCR7^+$Th17 cells. Black represents $CD4^+$ naïve T cells treated with DMSO; gray represents $CD4^+$ naïve T cells cocultured with NP-EVs-treated macrophages; blue represents $CD4^+$ naïve T cells co-cultured with PE-EVs-treated macrophages; red represents $CD4^+$ naïve T cells treated with BMS-754807 before co-cultured with PE-EVs-treated macrophages (n=10 in each group).

(E) Schematic of mice transferred $CD4^+$ T cells treated with BMS-754807 or PBS. Anti-CD4 antibody was used to deplete $CD4^+$ T cells in mice on day 10.5 of gestation. $CD4^+$ T cells were transferred into mice on day 11.5 of gestation. 20 μg/kg lipopolysaccharide (LPS) was intraperitoneally injected on day 12.5 and 15.5 of gestation to induce a PE-like pregnant mice model. Mice were sacrificed on day 18.5 of gestation.

(F) Embryo abortion rate of pregnant mice, body weight and crown-rump length of pups were measured on day 18.5 of gestation. Black represents the control group mice (n=6); gray represents mice treated with LPS (20μg/kg) to construct an animal model of PE (n=6); blue represents anti-CD4 antibody treated PE mice (n=6); red represents anti-CD4 antibody treated PE mice injected with $CD4^+$ T cells with DMSO treatment (n=7); orange represents anti-CD4 antibody treated PE mice injected with $CD4^+$ T cells with BMS754807 treatment (n=7).

(G) SBP and UACR of pregnant mice in the five groups.

(H) The frequencies of $CD4^+$ $CD44^+$ $IL\text{-}17A^+$ cells analyzed by flow cytometry.

Data were compared between groups using one-way ANOVA and represented as mean±SEM (*$P < 0.05$, ** $P < 0.01$, *** $P < 0.001$).

Figure 7—figure supplement 1 Cell–cell communications in immune cells when pro-inflam Macs accumulated at the maternal–fetal interface.

(A) Abundance of connections between different cell types at the maternal-fetal interface analyzed by CellPhoneDB.

(B) Capacities for interactions between immune cells are showed. Each line indicates the ligands expressed by the cell population represented by the same color (labeled). The lines connect to cell types that express cognate receptors. Line thickness is proportional to the number of ligands when cognate receptors are present in the recipient cell type.

1359 **Tables**

1360 **Table 1 Details of the individuals included in the CyTOF**

Parameters	NP (n=9)	PE (n=8)	GDM (n=8)	GDM&PE (n=7)	p Value
Age (years)	31.33 ± 2.108	31.75 ± 4.206	35.25 ±3.419	32.43 ± 2.321	0.1008
BMI (kg/m^2)	27.35 ± 1.740	30.84 ±2.888	29.56 ± 2.689	30.16 ± 2.280	0.0518
Gestational age (weeks)	38.89 ± 0.558	37.39 ± 1.253	38.73 ± 0.419	36.22 ± 1.372	<0.001
Number of living children	0.4444 ± 0.497	0.500 ± 0.500	1.125 ± 0.331	0.429 ± 0.495	0.0236
Previous abortions	0.7778 ± 1.030	1.000 ± 0.866	1.000 ± 1.000	1.714 ± 2.050	0.5848
Mean Systolic Blood Pressure	109.7 ± 5.400	151 ± 7.225	106.9 ± 2.848	150.7 ± 9.161	<0.0001

1361

1362 **Table 2 CyTOF antibody panel used for analyzing placentas from individuals with**
1363 **normal pregnancy (NP), preeclampsia (PE), gestational diabetes mellitus (GDM) and**
1364 **GDM complicated with PE (GDM&PE)**

Target	Metal tag
CD45	HI30
CD3	UCHT1
CD68	Y1/82A
CD56	NCAM16.2
gd TCR	5A6.E9
CD19	HIB19
CCR6	G034E3
CD38	HIT2
CD103	B-Ly7
CD39	A1
CXCR3	G025H7
PD-L1	29E.2A3
PD-1	EH12.2H7
CD11C	BU15
CD107a	H4A3
pAKT	D9E
CCR4	L291H4
TIGIT	A15153G
CD206	15-2
Helios	22F6
CD28	CD28.2
pSTAT3	4/p-Stat3
GITR	110416
CD33	WM53
CTLA-4	BN13
FOXP3	PCH101
CD163	GHI/61
CD45RA	HI100
ICOS	C398.4A
CD69	FN50
CCR7	G043H7
NKG2A	131411

CD15	W6D3
TIM-3	F38-2E2
CD86	Fun-1
HLA-DR	L243
Granzyme B	QA16A02
CD14	M5E2
pS6	A17020B
CD127	A019D5
CD4	RPA-T4
CD8	RPA-T8
CD11b	M1/70

1365

1366 **Table 3 Expression levels of markers identified in each immune subset in the placentas**

	B cells	$CD4^+$ T	$CD8^+$ T	gdTCR	NK cells	Macrophage	Granulocyte	MDSC	Dendritic cells
CD45	++	++	++	++	++	++	++	++	++
CD3	-	++	++	-	-	-	-	-	-
CD68	+	+	+	+	+	++	+	++	++
CD56	-	-	-	-	+	-	-	-	-
gd TCR	++	-	-	++	-	-	-	-	-
CD19	++	-	-	++	-	-	-	-	-
CCR6	+	-	-	-	-	-	-	-	-
CD38	++	++	+	+	++	++	-	-	+
CD103	-	-	-	-	-	-	-	-	-
CD39	++	-	-	-	+	++	+	+	+
CXCR3	+	+	+	+	+	+	-	+	++
PD-L1	-	-	-	-	-	-	-	+	-
PD-1	-	-	-	-	-	-	-	-	-
CD11C	+	-	-	-	+	++	++	+	++
CD107a	+	-	-	-	-	+	-	+	+
pAKT	+	+	+	+	+	++	+	+	+
CCR4	-	-	-	-	-	-	-	-	-
TIGIT	-	-	-	-	-	-	-	-	-
CD206	-	-	-	-	-	+	-	+	-
Helios	+	+	+	+	+	+	+	+	+
CD28	-	+	+	+	-	-	-	-	-
pSTAT3	+	+	-	+	-	+	+	-	-
GITR	-	-	-	-	-	-	-	-	-
CD33	-	-	-	-	-	+	-	+	-
CTLA-4	-	-	-	-	-	-	-	-	-
FOXP3	-	-	-	-	-	-	-	-	-
CD163	-	-	-	-	-	-	-	-	-
CD45RA	++	+	+	+	++	-	-	-	-
ICOS	-	+	+	-	-	-	-	-	-
CD69	+	+	+	+	++	+	-	++	-
CCR7	+	++	+	+	-	-	-	+	-
NKG2A	-	-	-	-	-	-	-	-	-
CD15	-	-	-	-	-	-	++	-	-
TIM-3	-	-	-	-	-	-	-	-	-

CD86	-	-	-	-	-	++	-	-	+
HLA-DR	++	-	+	+	-	++	+	-	++
Granzyme	+	-	-	+	++	+	+	-	-
CD14	-	-	-	-	-	++	-	-	-
pS6	-	-	-	-	-	-	-	-	-
CD127	-	++	+	-	-	-	-	-	-
CD4	-	++	-	-	-	-	-	-	-
CD8	-	-	++	-	-	-	-	-	-
CD11b	-	-	-	+	+	++	++	-	+

Table 4 The marker profile of PE-specific immune subsets

	memory-like $CD4^+$ T cells	memory-like $CD8^+$ T cells	gMDSCs	pro-inflammatory macrophages	anti-inflammatory macrophages
	Cluster 08 of $CD4^+$ T cells	Cluster 02 of $CD8^+$ T cells	Cluster 12 of $CD3^-CD11b^+$ cells	Cluster 23 of $CD3^-CD11b^+$ cells	Cluster 25 of $CD3^-CD11b^+$ cells
CD45	++	++	++	++	++
CD3	++	++	-	-	-
CD68	-	-	+	++	++
CD56	-	-	-	-	-
gd TCR	-	-	-	-	-
CD19	-	-	-	-	-
CCR6	-	-	-	-	-
CD38	++	++	-	+	+
CD103	-	-	-	+	+
CD39	+	-	+	-	-
CXCR3	+	+	-	-	-
PD-L1	-	-	-	-	-
PD-1	-	-	-	-	-
CD11C	-	-	++	++	++
CD107a	-	-	-	+	+
pAKT	+	+	-	-	-
CCR4	-	-	-	-	-
TIGIT	-	-	-	-	-
CD206	-	-	+	-	+
Helios	+	+	-	-	-
CD28	+	+	-	-	-
pSTAT3	-	-	-	-	-
GITR	-	-	-	-	-
CD33	-	-	-	-	+
CTLA-4	-	-	-	-	-
FOXP3	-	-	-	-	-
CD163	-	-	-	-	-
CD45RA	-	-	-	-	-
ICOS	+	+	-	-	-
CD69	+	-	-	-	-
CCR7	++	++	-	-	-
NKG2A	-	-	-	-	-
CD15	-	-	++	-	-

TIM-3	-	-	-	-	-
CD86	-	-	-	+	+
HLA-DR	-	-	+	+	++
Granzyme B	-	-	+	-	-
CD14	-	-	-	+	+
pS6	-	-	-	-	-
CD127	+	-	-	-	-
CD4	++	-	-	-	-
CD8	-	++	-	-	-
CD11b	-	-	++	++	++

1369

1370 **Table 5 Details of the individual with NP or PE included in the study**

Parameters	NP (n=30)	PE (n=30)	p Value
Age (years)	31.13 ± 2.9747	31.50 ± 4.1693	0.0741
BMI (kg/m^2)	27.24 ± 2.8048	29.48±3.9295	0.0155
Gestational age (weeks)	38.68± 0.6038	35.53 ± 3.29	<0.0001
Number of living children	0.6000 ± 0.4900	0.4667 ± 0.6182	0.3665

1371

1372 **Table 6 Details of the individual with early-onset preeclampsia or late-onset**
1373 **preeclampsia included in the study**

Parameters	Early-onset preeclampsia (n=11)	Late-onset preeclampsia (n=19)	p Value
The gestational week when blood pressure begins to rise	28.82± 2.8220	36.05± 1.129	< 0.0001
Age (years)	32.45± 4.6768	32.36± 3.8472	0.9568
BMI (kg/m^2)	29.64± 2.6840	28.71±4.4506	0.5388
Gestational age (weeks)	33.45± 3.7887	36.77± 1.2171	0.0014
Number of living children	0.36± 0.5045	0.36 ± 0.4956	0.98

1374

1375

Figure 1

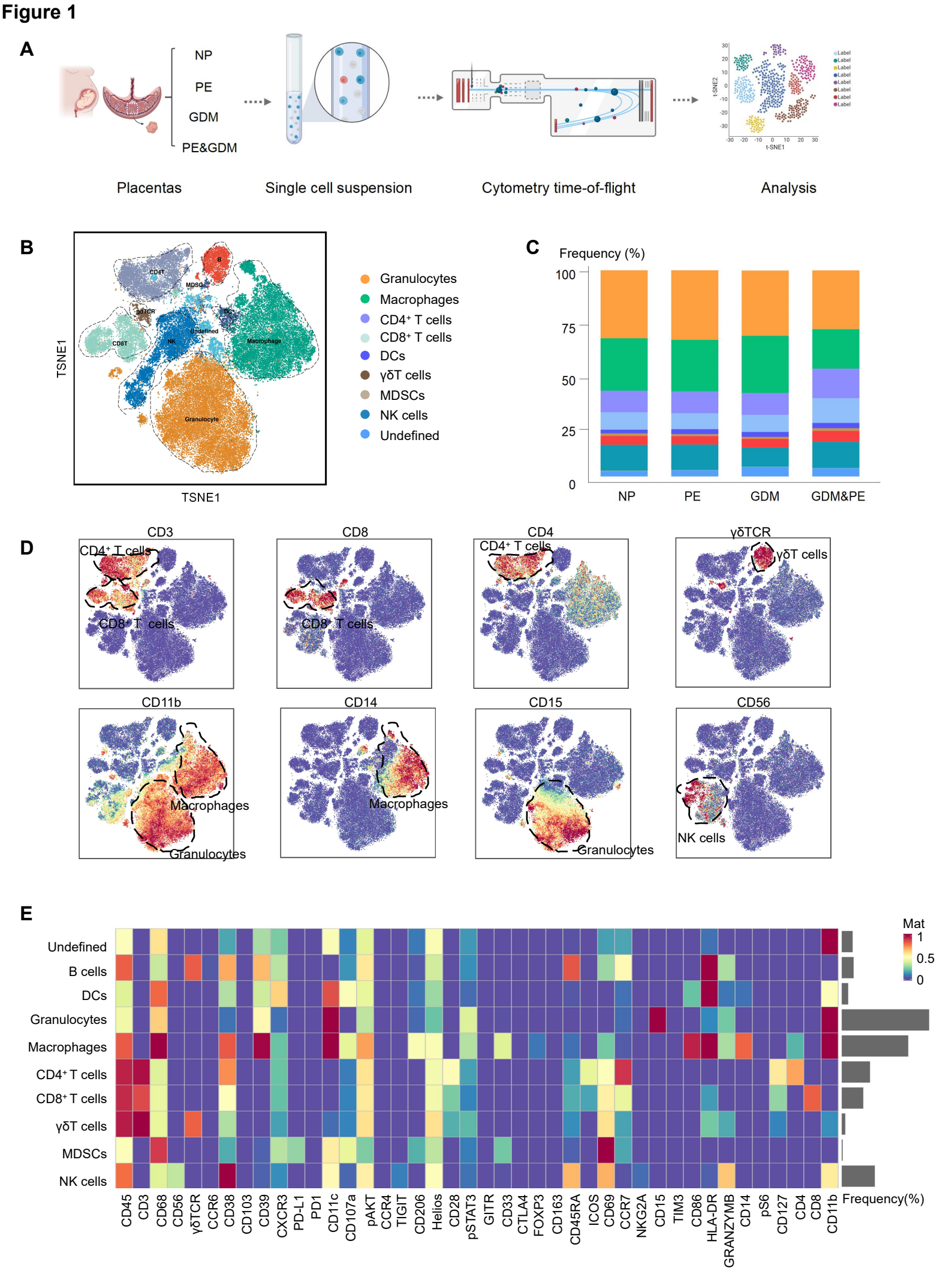
A
NP
PE
GDM
PE&GDM
Placentas
Single cell suspension
Cytometry time-of-flight
Analysis
B
TSNE1
TSNE1
Granulocytes
Macrophages
CD4⁺ T cells
CD8⁺ T cells
DCs
γδT cells
MDSCs
NK cells
Undefined
C
Frequency (%)
100
75
50
25
0
NP
PE
GDM
GDM&PE
D
CD3
CD4⁺ T cells
CD8⁺ T cells
CD8
CD8⁺ T cells
CD4
CD4⁺ T cells
γδTCR
γδT cells
CD11b
Macrophages
Granulocytes
CD14
Macrophages
CD15
Granulocytes
CD56
NK cells
E
Undefined
B cells
DCs
Granulocytes
Macrophages
CD4⁺ T cells
CD8⁺ T cells
γδT cells
MDSCs
NK cells
CD45
CD3
CD68
CD56
γδTCR
CCR6
CD38
CD103
CD39
CXCR3
PD-L1
PD1
CD11c
CD107a
pAKT
CCR4
TIGIT
CD206
Helios
CD28
pSTAT3
GITR
CD33
CTLA4
FOXP3
CD163
CD45RA
ICOS
CD69
CCR7
NKG2A
CD15
TIM3
CD86
HLA-DR
GRANZYMB
CD14
pS6
CD127
CD4
CD8
CD11b
Frequency(%)
Mat
1
0.5
0

Figure 2

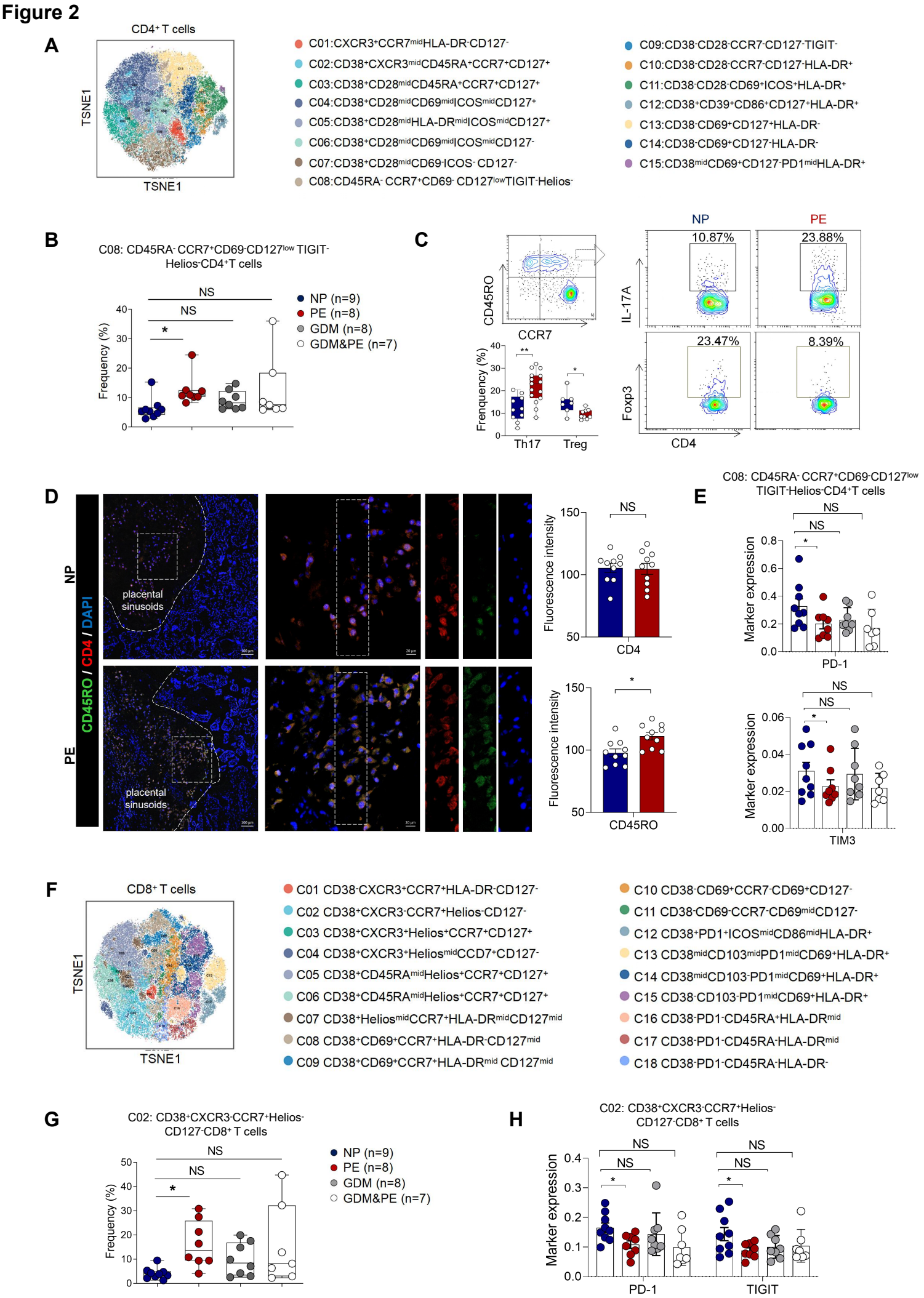
A
CD4+ T cells
TSNE1
TSNE1
C01:CXCR3+CCR7midHLA-DR-CD127-
C02:CD38+CXCR3midCD45RA+CCR7+CD127+
C03:CD38+CD28midCD45RA+CCR7+CD127+
C04:CD38+CD28midCD69midICOSmidCD127+
C05:CD38+CD28midHLA-DRmidICOSmidCD127+
C06:CD38+CD28midCD69midICOSmidCD127-
C07:CD38+CD28midCD69-ICOS- CD127-
C08:CD45RA- CCR7+CD69- CD127lowTIGIT-Helios-
C09:CD38-CD28-CCR7-CD127-TIGIT-
C10:CD38-CD28-CCR7-CD127-HLA-DR+
C11:CD38-CD28-CD69+ICOS+HLA-DR+
C12:CD38+CD39+CD86+CD127+HLA-DR+
C13:CD38-CD69+CD127+HLA-DR-
C14:CD38-CD69+CD127-HLA-DR-
C15:CD38midCD69+CD127-PD1midHLA-DR+
B
C08: CD45RA- CCR7+CD69-CD127low TIGIT-
Helios-CD4+T cells
NS
NS
*
Frequency (%)
NP (n=9)
PE (n=8)
GDM (n=8)
GDM&PE (n=7)
C
CD45RO
CCR7
Frenquency (%)
**
*
Th17
Treg
NP
PE
10.87%
23.88%
23.47%
8.39%
IL-17A
Foxp3
CD4
D
NP
PE
CD45RO / CD4 / DAPI
placental sinusoids
placental sinusoids
Fluorescence intensity
NS
CD4
*
CD45RO
E
C08: CD45RA- CCR7+CD69-CD127low
TIGIT-Helios-CD4+T cells
NS
NS
*
Marker expression
PD-1
NS
NS
*
Marker expression
TIM3
F
CD8+ T cells
TSNE1
TSNE1
C01 CD38-CXCR3+CCR7+HLA-DR-CD127-
C02 CD38+CXCR3-CCR7+Helios-CD127-
C03 CD38+CXCR3+Helios+CCR7+CD127+
C04 CD38+CXCR3+HeliosmidCCD7+CD127-
C05 CD38+CD45RAmidHelios+CCR7+CD127+
C06 CD38+CD45RAmidHelios+CCR7+CD127+
C07 CD38+HeliosmidCCR7+HLA-DRmidCD127mid
C08 CD38+CD69+CCR7+HLA-DR-CD127mid
C09 CD38+CD69+CCR7+HLA-DRmid CD127mid
C10 CD38-CD69+CCR7-CD69+CD127-
C11 CD38-CD69-CCR7-CD69midCD127-
C12 CD38+PD1+ICOSmidCD86midHLA-DR+
C13 CD38midCD103midPD1midCD69+HLA-DR+
C14 CD38midCD103-PD1midCD69+HLA-DR+
C15 CD38-CD103-PD1midCD69+HLA-DR+
C16 CD38-PD1-CD45RA+HLA-DRmid
C17 CD38-PD1-CD45RA-HLA-DRmid
C18 CD38-PD1-CD45RA-HLA-DR-
G
C02: CD38+CXCR3-CCR7+Helios-
CD127-CD8+ T cells
NS
NS
*
Frequency (%)
NP (n=9)
PE (n=8)
GDM (n=8)
GDM&PE (n=7)
H
C02: CD38+CXCR3-CCR7+Helios-
CD127-CD8+ T cells
NS
NS
*
NS
NS
*
Marker expression
PD-1
TIGIT

Figure 2 figure supplement 1

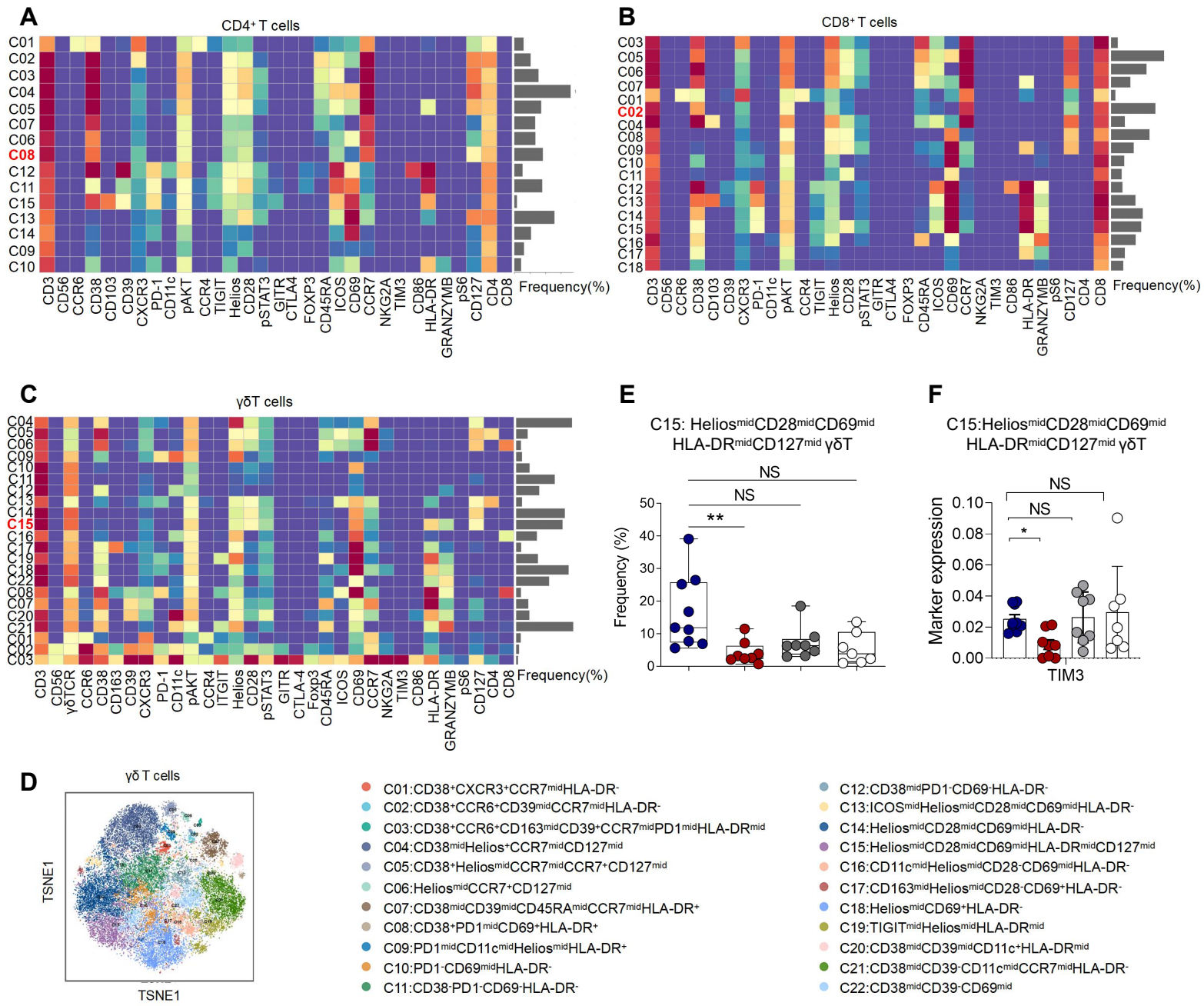

Figure 3

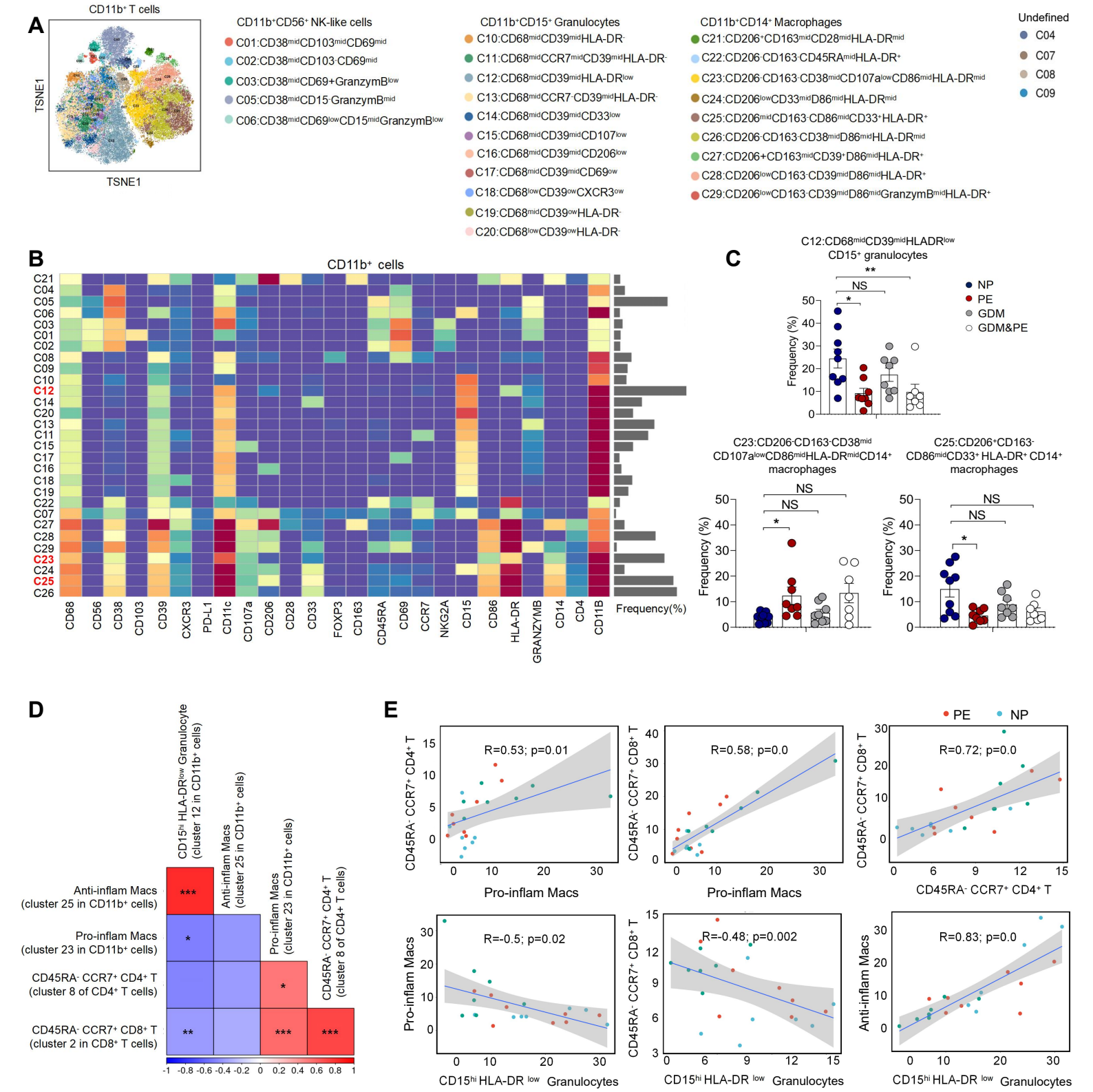
A
CD11b+ T cells
TSNE1
TSNE1
CD11b+CD56+ NK-like cells
C01:CD38midCD103midCD69mid
C02:CD38midCD103-CD69mid
C03:CD38midCD69+GranzymBlow
C05:CD38midCD15-GranzymBmid
C06:CD38midCD69lowCD15midGranzymBlow
CD11b+CD15+ Granulocytes
C10:CD68midCD39midHLA-DR-
C11:CD68midCCR7midCD39midHLA-DR-
C12:CD68midCD39midHLA-DRlow
C13:CD68midCCR7-CD39midHLA-DR-
C14:CD68midCD39midCD33low
C15:CD68midCD39midCD107low
C16:CD68midCD39midCD206low
C17:CD68midCD39midCD69ow
C18:CD68lowCD39owCXCR3ow
C19:CD68midCD39owHLA-DR-
C20:CD68lowCD39owHLA-DR-
CD11b+CD14+ Macrophages
C21:CD206+CD163midCD28midHLA-DRmid
C22:CD206-CD163-CD45RAmidHLA-DR+
C23:CD206-CD163-CD38midCD107alowCD86midHLA-DRmid
C24:CD206lowCD33midD86midHLA-DRmid
C25:CD206midCD163-CD86midCD33+HLA-DR+
C26:CD206-CD163-CD38midD86midHLA-DRmid
C27:CD206+CD163midCD39+D86midHLA-DR+
C28:CD206lowCD163-CD39midD86midHLA-DR+
C29:CD206lowCD163-CD39midD86midGranzymBmidHLA-DR+
Undefined
C04
C07
C08
C09
B
CD11b+ cells
C21
C04
C05
C06
C03
C01
C02
C08
C09
C10
C12
C14
C20
C13
C11
C15
C17
C16
C18
C19
C22
C07
C27
C28
C29
C23
C24
C25
C26
CD68
CD56
CD38
CD103
CD39
CXCR3
PD-L1
CD11c
CD107a
CD206
CD28
CD33
FOXP3
CD163
CD45RA
CD69
CCR7
NKG2A
CD15
CD86
HLA-DR
GRANZYMB
CD14
CD4
CD11B
Frequency(%)
C
C12:CD68midCD39midHLADRlow
CD15+ granulocytes
NP
PE
GDM
GDM&PE
Frequency (%)
NS
*
**
C23:CD206-CD163-CD38mid
CD107alowCD86midHLA-DRmidCD14+
macrophages
C25:CD206+CD163-
CD86midCD33+ HLA-DR+ CD14+
macrophages
D
CD15hi HLA-DRlow Granulocyte
(cluster 12 in CD11b+ cells)
Anti-inflam Macs
(cluster 25 in CD11b+ cells)
Pro-inflam Macs
(cluster 23 in CD11b+ cells)
CD45RA- CCR7+ CD4+ T
(cluster 8 of CD4+ T cells)
CD45RA- CCR7+ CD8+ T
(cluster 2 in CD8+ T cells)
***
*
**
-1 -0.8 -0.6 -0.4 -0.2 0 0.2 0.4 0.6 0.8 1
E
PE
NP
R=0.53; p=0.01
R=0.58; p=0.0
R=0.72; p=0.0
R=-0.5; p=0.02
R=-0.48; p=0.002
R=0.83; p=0.0
CD45RA- CCR7+ CD4+ T
CD45RA- CCR7+ CD8+ T
Pro-inflam Macs
Anti-inflam Macs
CD15hi HLA-DR low Granulocytes

Figure 4

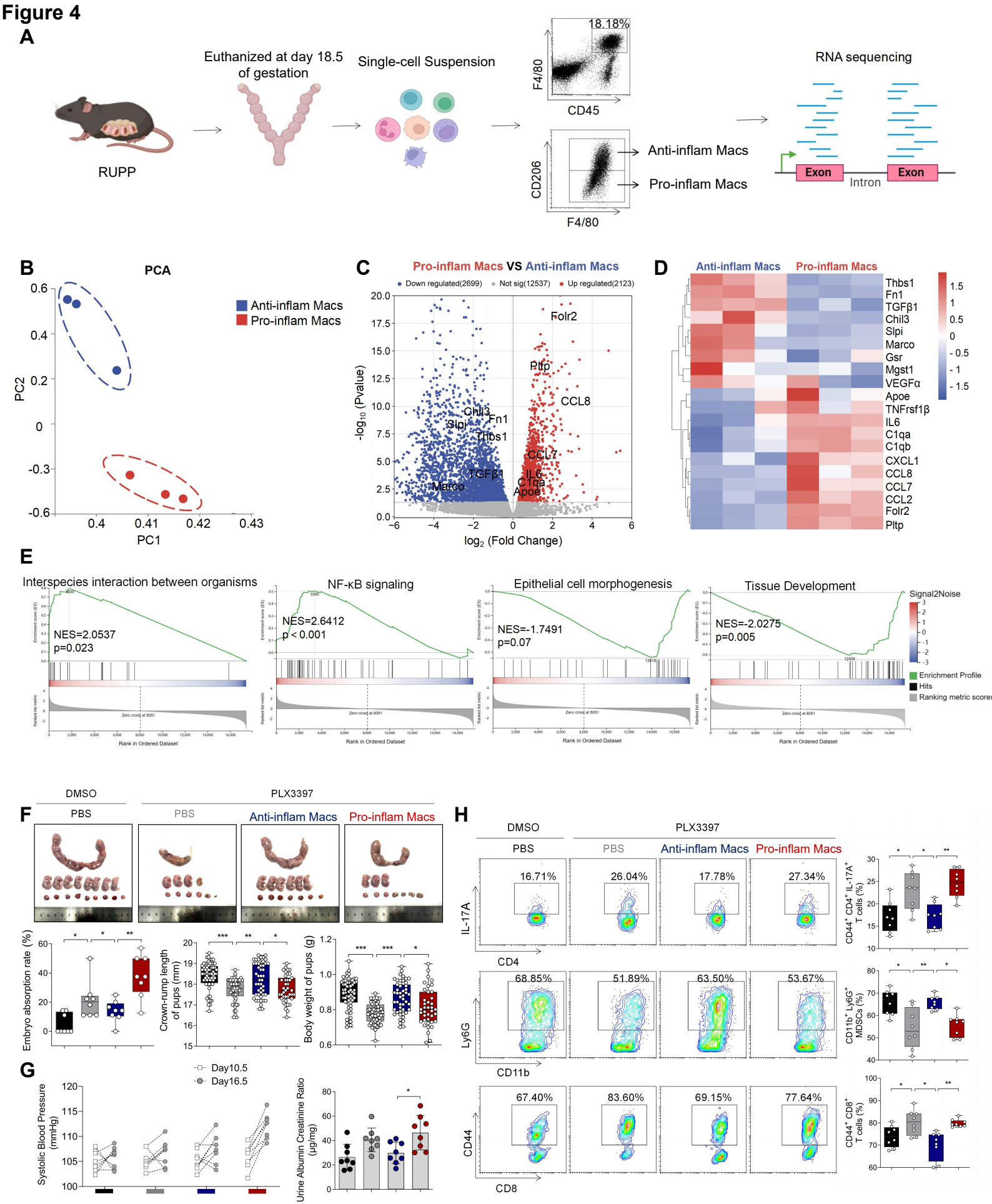
A
RUPP
Euthanized at day 18.5 of gestation
Single-cell Suspension
18.18%
F4/80
CD45
CD206
F4/80
Anti-inflam Macs
Pro-inflam Macs
RNA sequencing
Exon
Intron
Exon
B
PCA
Anti-inflam Macs
Pro-inflam Macs
PC2
PC1
C
Pro-inflam Macs VS Anti-inflam Macs
Down regulated(2699)
Not sig(12537)
Up regulated(2123)
-log10 (Pvalue)
log2 (Fold Change)
Folr2
Pltp
CCL8
Chil3
Fn1
Slpi
Thbs1
CCL7
TGFβ1
IL6
C1qa
Marco
Apoe
D
Anti-inflam Macs
Pro-inflam Macs
Thbs1
Fn1
TGFβ1
Chil3
Slpi
Marco
Gsr
Mgst1
VEGFα
Apoe
TNFrsf1β
IL6
C1qa
C1qb
CXCL1
CCL8
CCL7
CCL2
Folr2
Pltp
E
Interspecies interaction between organisms
NES=2.0537
p=0.023
NF-κB signaling
NES=2.6412
p < 0.001
Epithelial cell morphogenesis
NES=-1.7491
p=0.07
Tissue Development
NES=-2.0275
p=0.005
Signal2Noise
Enrichment Profile
Hits
Ranking metric scores
Rank in Ordered Dataset
F
DMSO
PLX3397
PBS
PBS
Anti-inflam Macs
Pro-inflam Macs
Embryo absorption rate (%)
Crown-rump length of pups (mm)
Body weight of pups (g)
G
Day10.5
Day16.5
Systolic Blood Pressure (mmHg)
Urine Albumin Creatinine Ratio (μg/mg)
H
DMSO
PLX3397
PBS
PBS
Anti-inflam Macs
Pro-inflam Macs
IL-17A
CD4
16.71%
26.04%
17.78%
27.34%
CD44+ CD4+ IL-17A+ T cells (%)
Ly6G
CD11b
68.85%
51.89%
63.50%
53.67%
CD11b+ Ly6G+ MDSCs (%)
CD44
CD8
67.40%
83.60%
69.15%
77.64%
CD44+ CD8+ T cells (%)

Figure 4 figure supplement 1

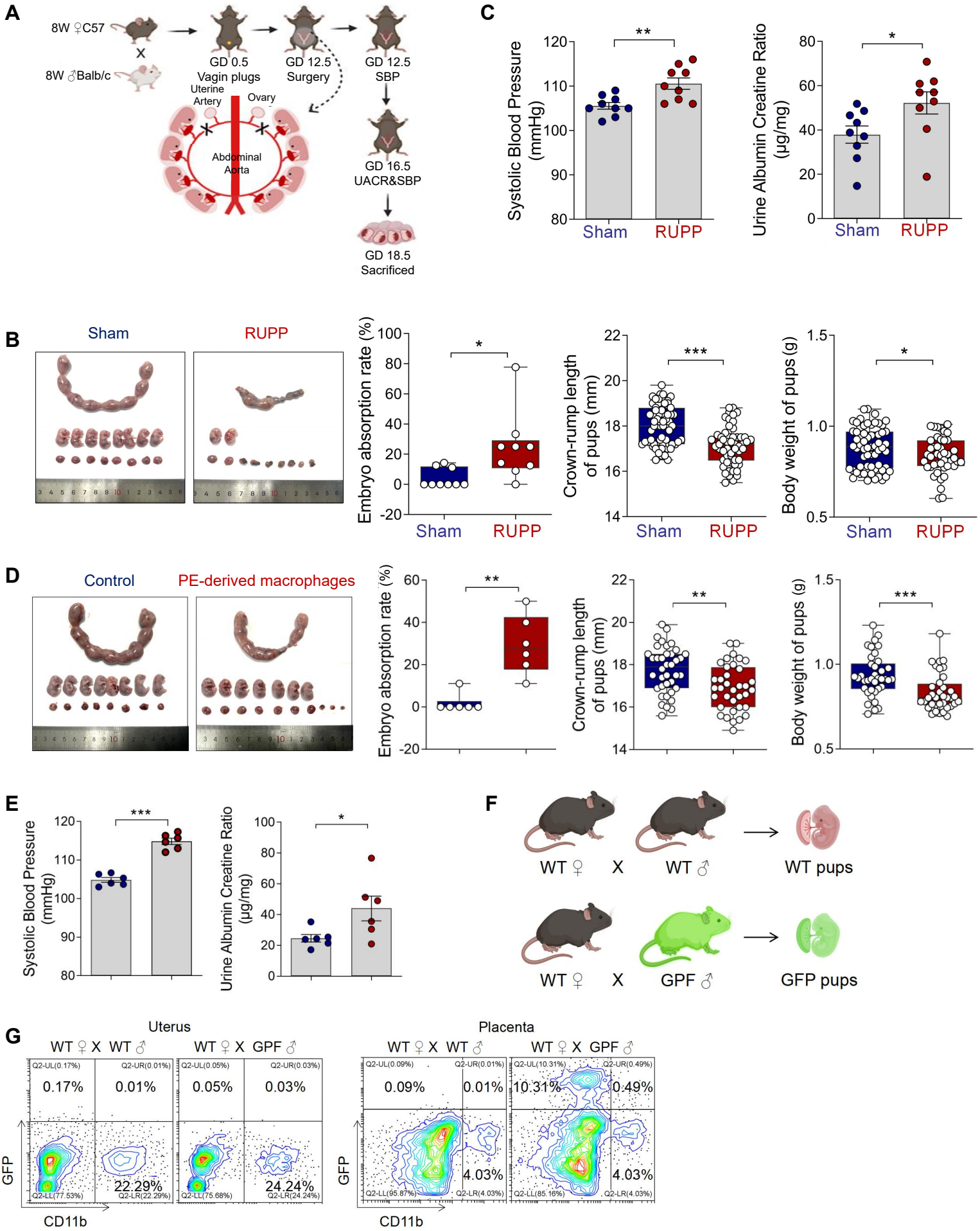

Figure 4 figure supplement 2

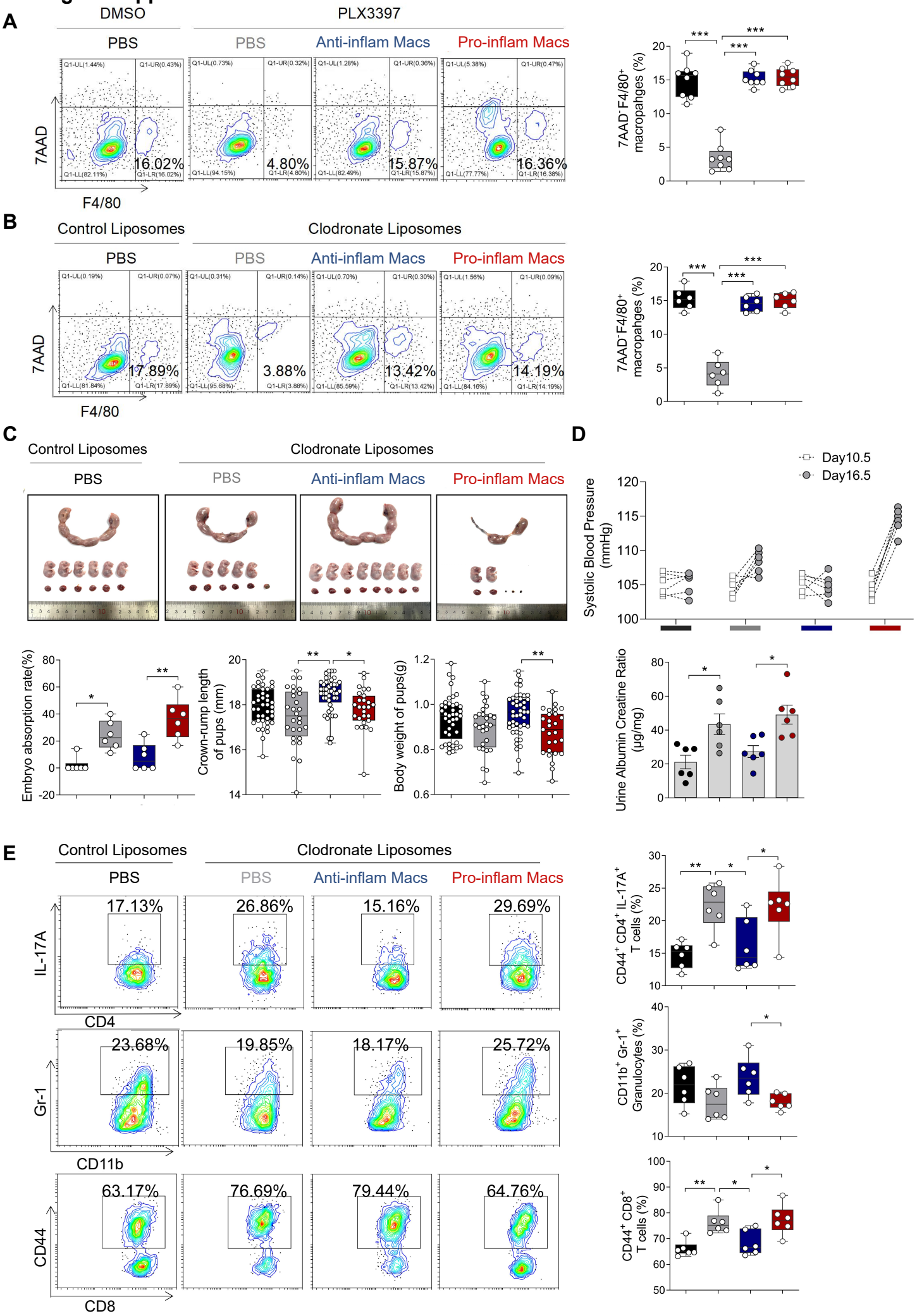

Figure 5

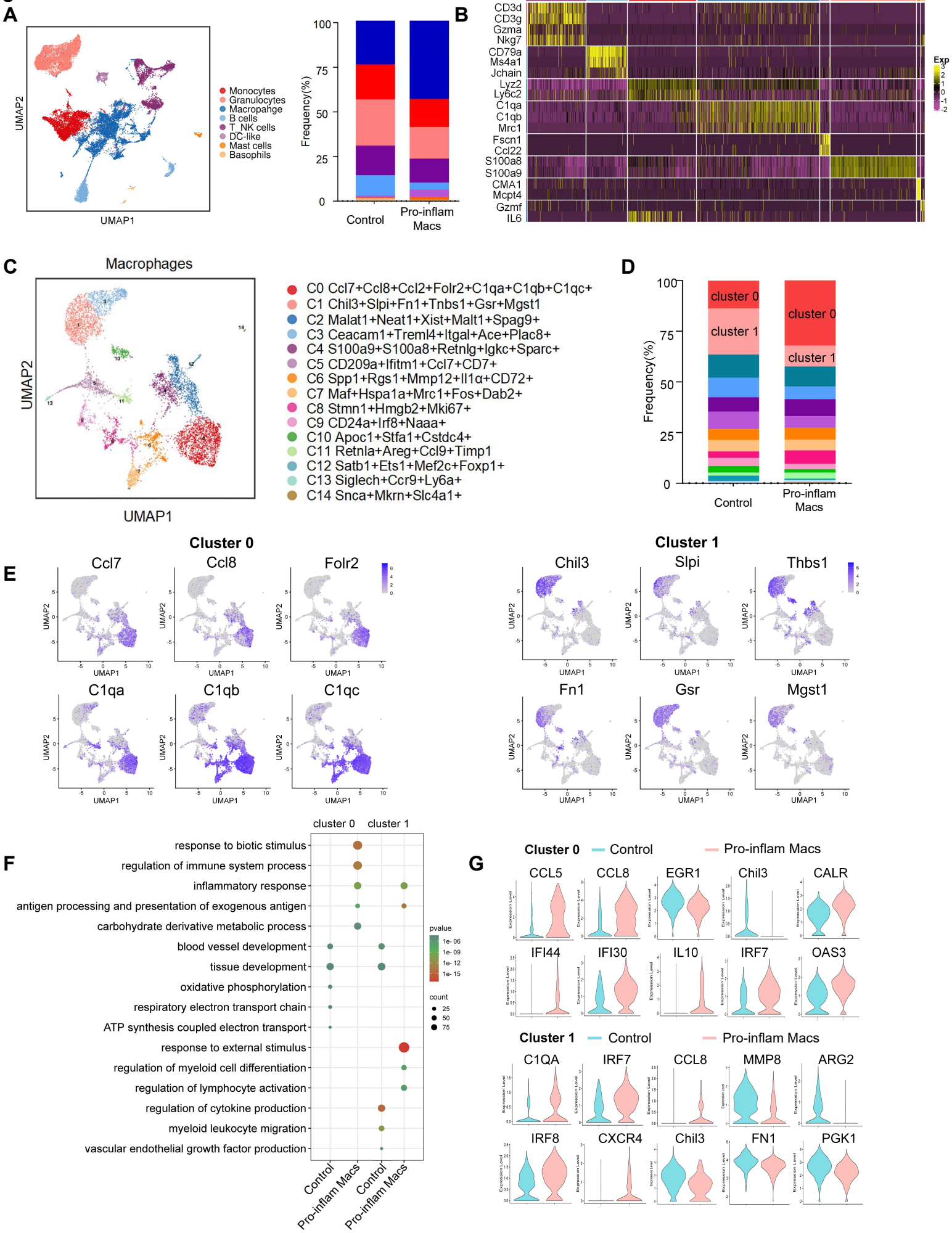
A
UMAP2
UMAP1
Monocytes
Granulocytes
Macropahge
B cells
T_NK cells
DC-like
Mast cells
Basophils
Frequency(%)
100
75
50
25
0
Control
Pro-inflam Macs
B
CD3d
CD3g
Gzma
Nkg7
CD79a
Ms4a1
Jchain
Lyz2
Ly6c2
C1qa
C1qb
Mrc1
Fscn1
Ccl22
S100a8
S100a9
CMA1
Mcpt4
Gzmf
IL6
Exp
C
Macrophages
UMAP2
UMAP1
C0 Ccl7+Ccl8+Ccl2+Folr2+C1qa+C1qb+C1qc+
C1 Chil3+Slpi+Fn1+Tnbs1+Gsr+Mgst1
C2 Malat1+Neat1+Xist+Malt1+Spag9+
C3 Ceacam1+Treml4+Itgal+Ace+Plac8+
C4 S100a9+S100a8+Retnlg+Igkc+Sparc+
C5 CD209a+Ifitm1+Ccl7+CD7+
C6 Spp1+Rgs1+Mmp12+Il1α+CD72+
C7 Maf+Hspa1a+Mrc1+Fos+Dab2+
C8 Stmn1+Hmgb2+Mki67+
C9 CD24a+Irf8+Naaa+
C10 Apoc1+Stfa1+Cstdc4+
C11 Retnla+Areg+Ccl9+Timp1
C12 Satb1+Ets1+Mef2c+Foxp1+
C13 Siglech+Ccr9+Ly6a+
C14 Snca+Mkrn+Slc4a1+
D
Frequency(%)
cluster 0
cluster 1
Control
Pro-inflam Macs
E
Cluster 0
Ccl7
Ccl8
Folr2
C1qa
C1qb
C1qc
Cluster 1
Chil3
Slpi
Thbs1
Fn1
Gsr
Mgst1
UMAP1
UMAP2
F
cluster 0
cluster 1
response to biotic stimulus
regulation of immune system process
inflammatory response
antigen processing and presentation of exogenous antigen
carbohydrate derivative metabolic process
blood vessel development
tissue development
oxidative phosphorylation
respiratory electron transport chain
ATP synthesis coupled electron transport
response to external stimulus
regulation of myeloid cell differentiation
regulation of lymphocyte activation
regulation of cytokine production
myeloid leukocyte migration
vascular endothelial growth factor production
Control
Pro-inflam Macs
pvalue
1e-06
1e-09
1e-12
1e-15
count
25
50
75
G
Cluster 0
Control
Pro-inflam Macs
CCL5
CCL8
EGR1
Chil3
CALR
IFI44
IFI30
IL10
IRF7
OAS3
Cluster 1
C1QA
IRF7
CCL8
MMP8
ARG2
IRF8
CXCR4
Chil3
FN1
PGK1
Expression Level

Figure 5 figure supplement 1

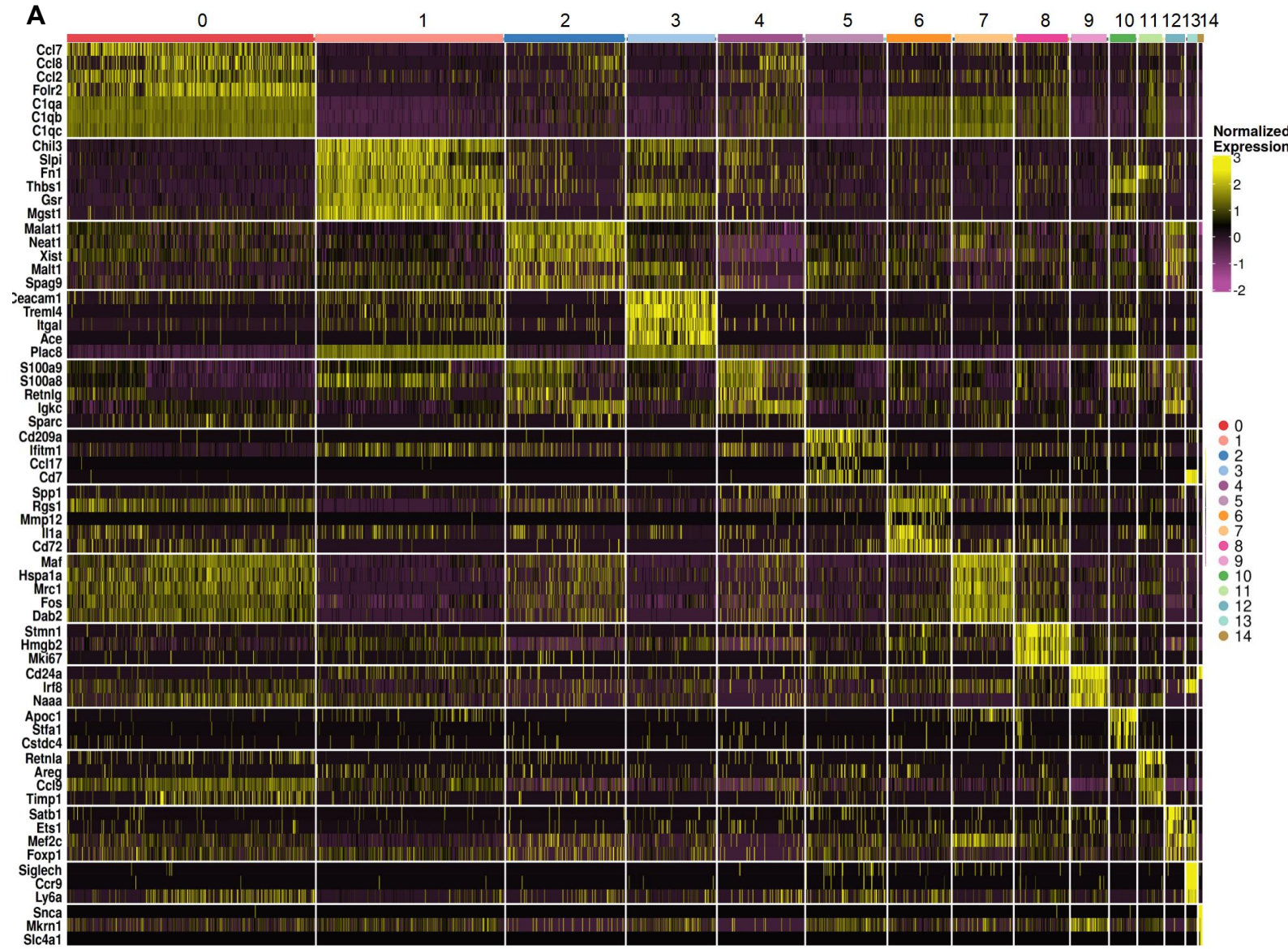

Figure 6

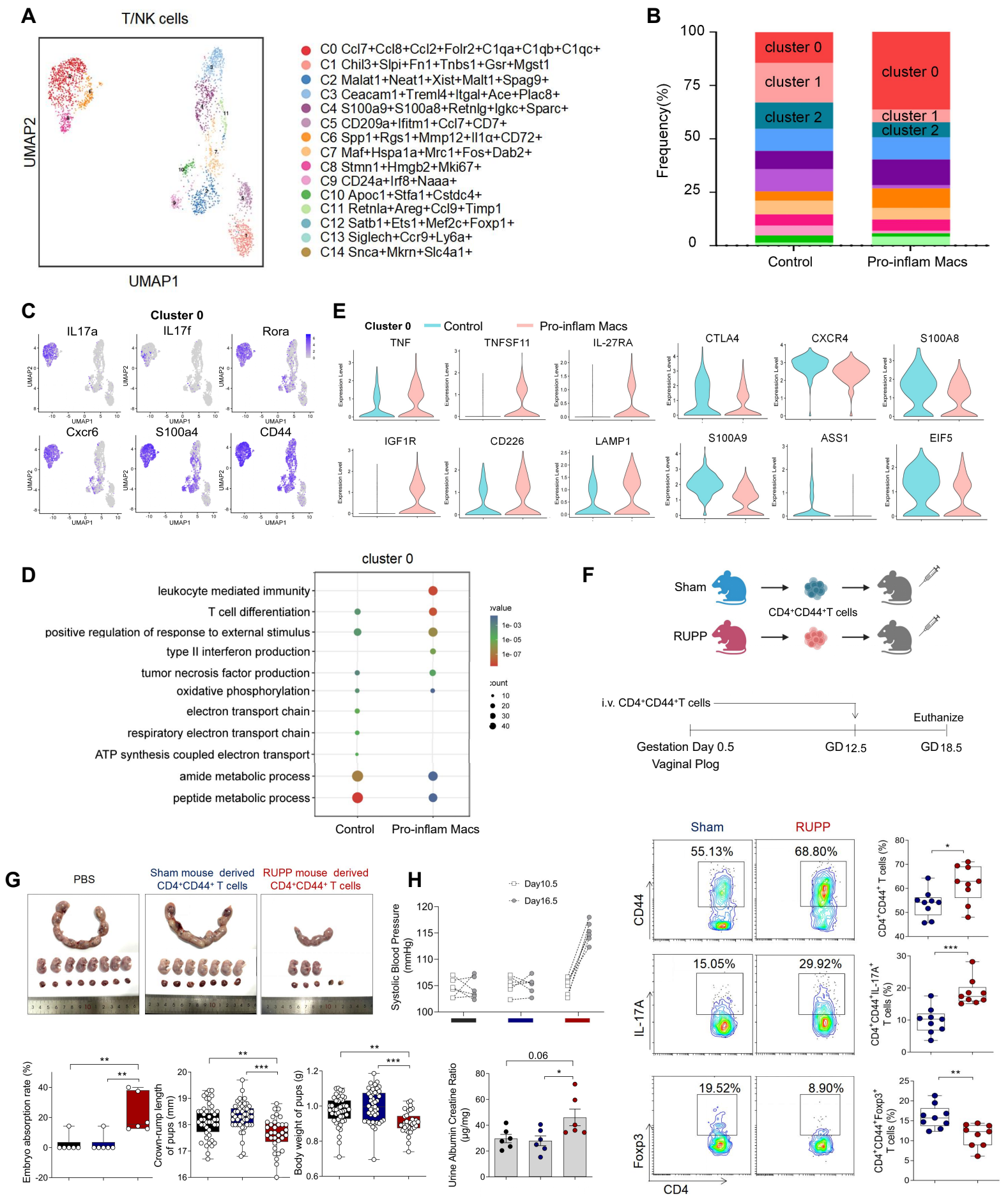
A
T/NK cells
UMAP2
UMAP1
C0 Ccl7+Ccl8+Ccl2+Folr2+C1qa+C1qb+C1qc+
C1 Chil3+Slpi+Fn1+Tnbs1+Gsr+Mgst1
C2 Malat1+Neat1+Xist+Malt1+Spag9+
C3 Ceacam1+Treml4+Itgal+Ace+Plac8+
C4 S100a9+S100a8+Retnlg+Igkc+Sparc+
C5 CD209a+Ifitm1+Ccl7+CD7+
C6 Spp1+Rgs1+Mmp12+Il1α+CD72+
C7 Maf+Hspa1a+Mrc1+Fos+Dab2+
C8 Stmn1+Hmgb2+Mki67+
C9 CD24a+Irf8+Naaa+
C10 Apoc1+Stfa1+Cstdc4+
C11 Retnla+Areg+Ccl9+Timp1
C12 Satb1+Ets1+Mef2c+Foxp1+
C13 Siglech+Ccr9+Ly6a+
C14 Snca+Mkrn+Slc4a1+
B
Frequency(%)
cluster 0
cluster 1
cluster 2
Control
Pro-inflam Macs
C
Cluster 0
IL17a
IL17f
Rora
Cxcr6
S100a4
CD44
E
Cluster 0
Control
Pro-inflam Macs
TNF
TNFSF11
IL-27RA
CTLA4
CXCR4
S100A8
IGF1R
CD226
LAMP1
S100A9
ASS1
EIF5
D
cluster 0
leukocyte mediated immunity
T cell differentiation
positive regulation of response to external stimulus
type II interferon production
tumor necrosis factor production
oxidative phosphorylation
electron transport chain
respiratory electron transport chain
ATP synthesis coupled electron transport
amide metabolic process
peptide metabolic process
Control
Pro-inflam Macs
F
Sham
RUPP
CD4+CD44+T cells
i.v. CD4+CD44+T cells
Euthanize
Gestation Day 0.5
Vaginal Plog
GD 12.5
GD 18.5
G
PBS
Sham mouse derived CD4+CD44+ T cells
RUPP mouse derived CD4+CD44+ T cells
Embryo absorption rate (%)
Crown-rump length of pups (mm)
Body weight of pups (g)
H
Day10.5
Day16.5
Systolic Blood Pressure (mmHg)
Urine Albumin Creatine Ratio (μg/mg)
0.06
Sham
RUPP
55.13%
68.80%
15.05%
29.92%
19.52%
8.90%
CD44
IL-17A
Foxp3
CD4
CD4+CD44+ T cells (%)
CD4+CD44+IL-17A+ T cells (%)
CD4+CD44+Foxp3+ T cells (%)

Figure 6 figure supplement 1

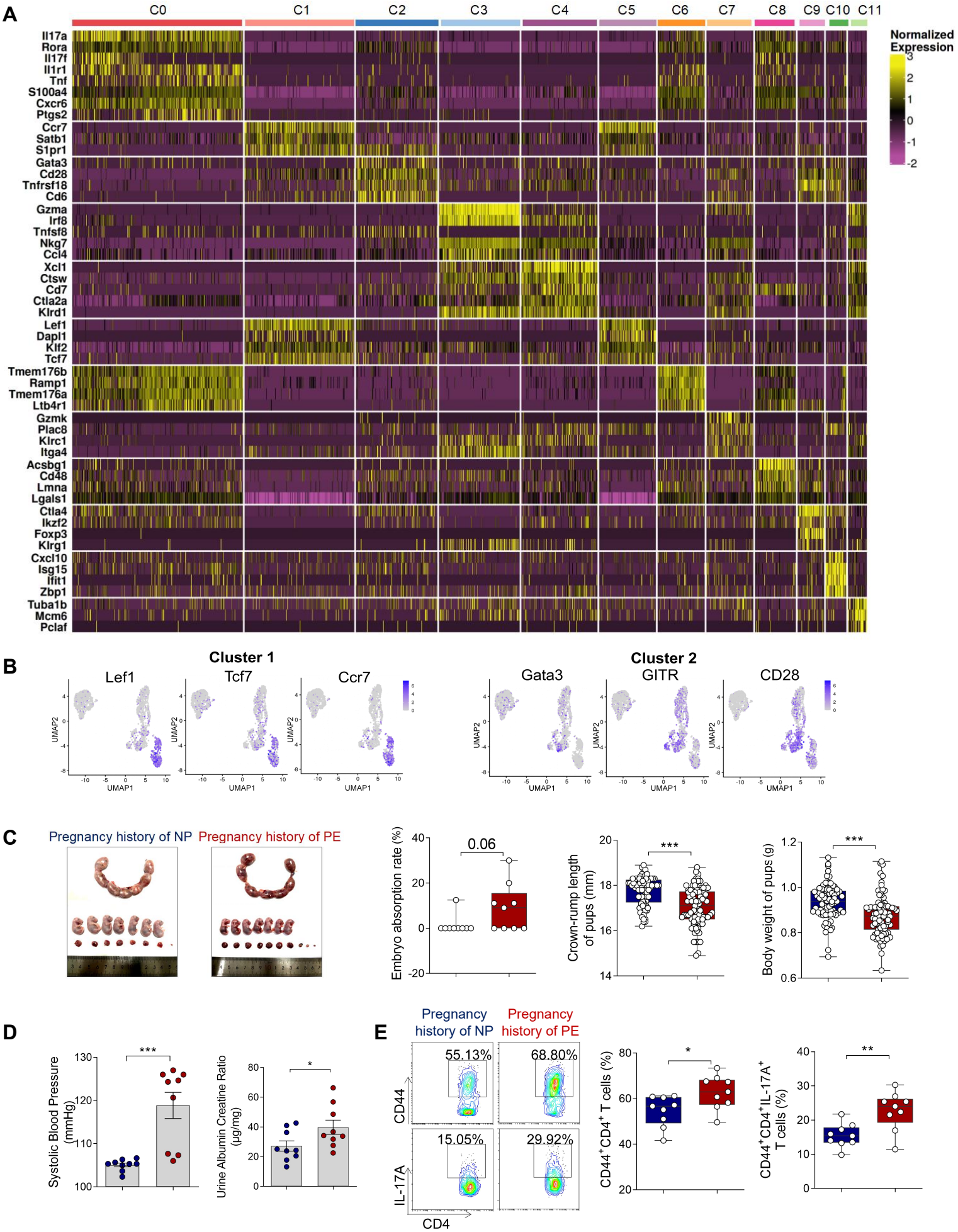

Figure 6 figure supplement 2

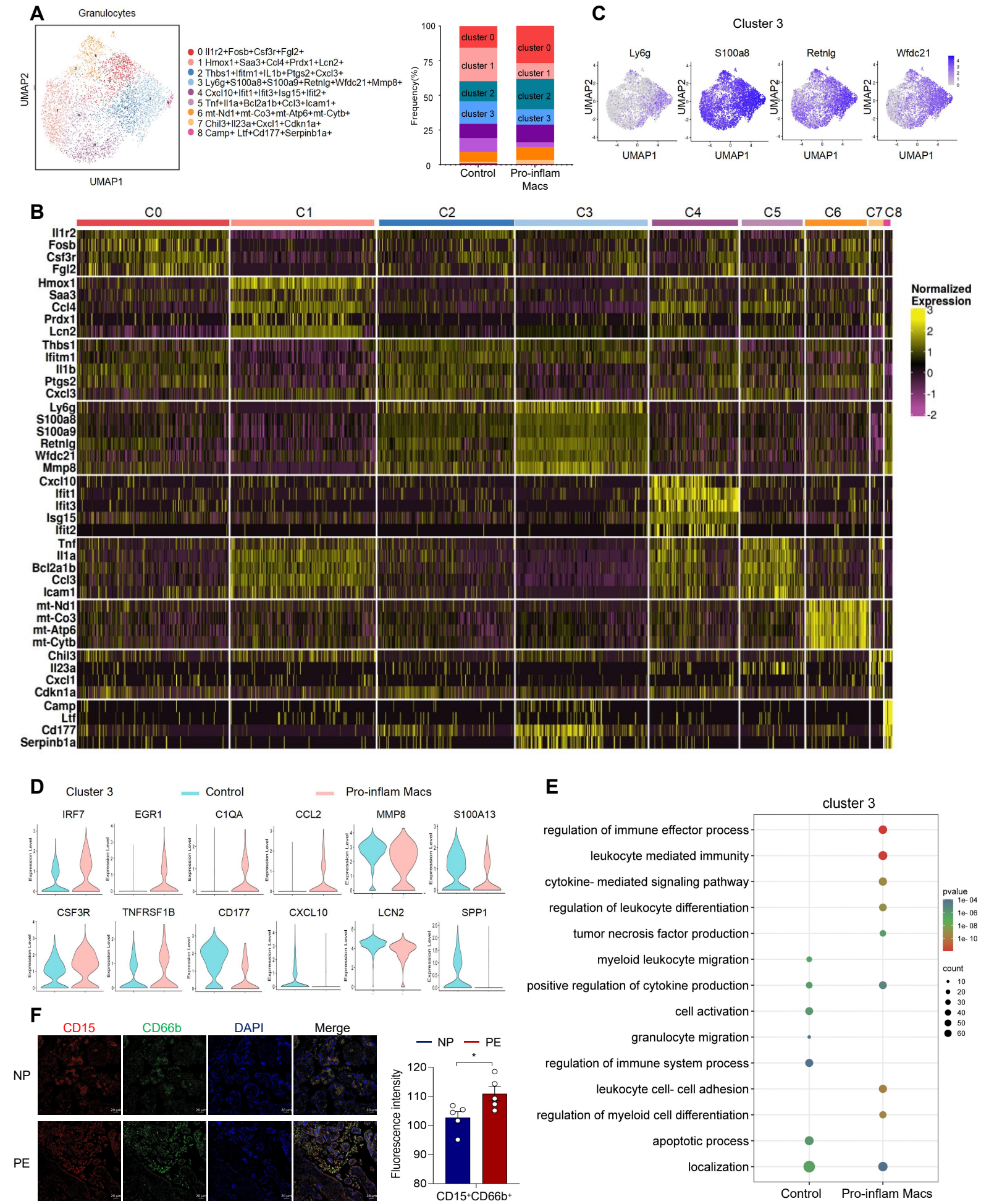

Figure 7

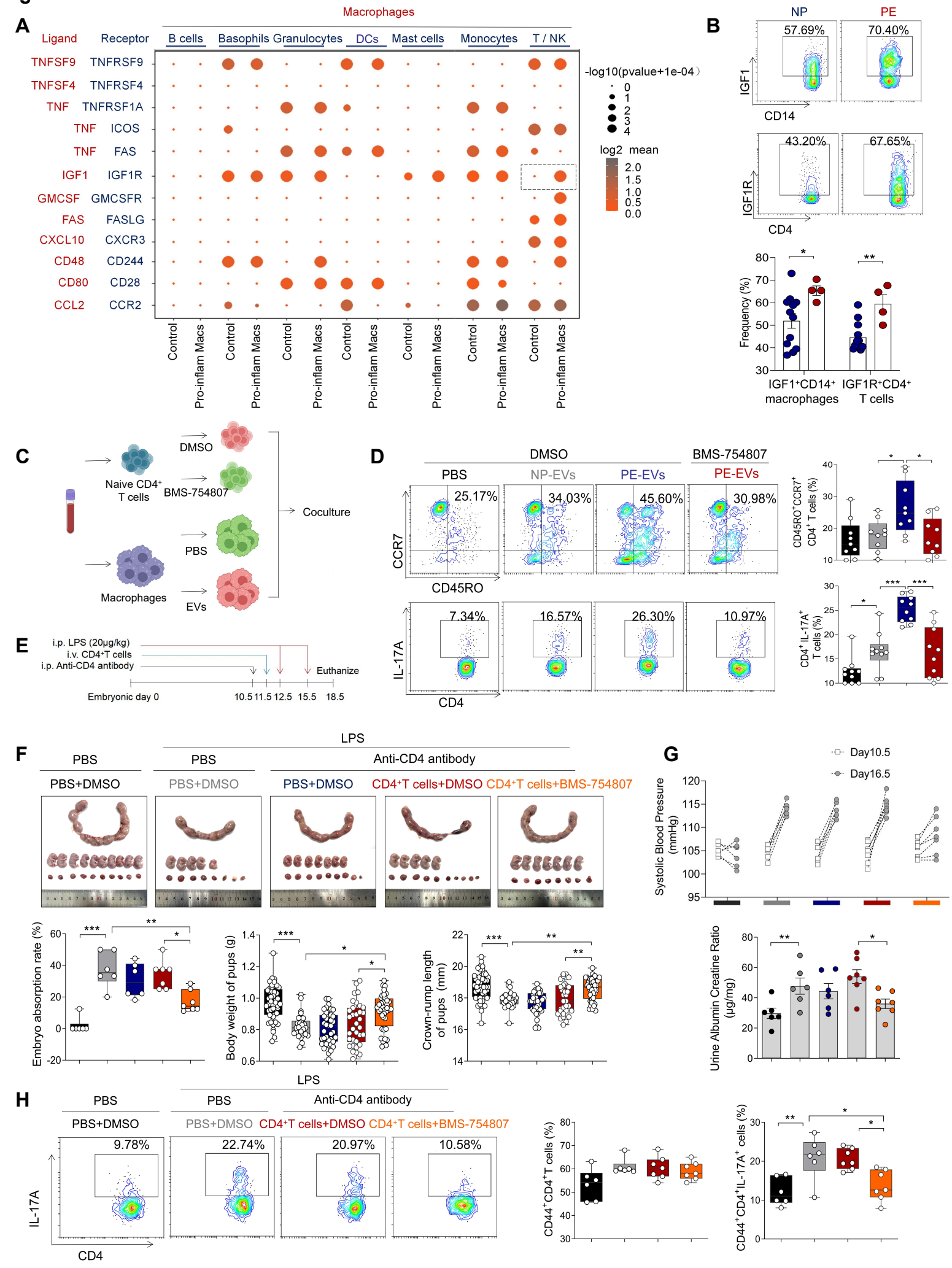
A
Macrophages
Ligand
Receptor
B cells
Basophils
Granulocytes
DCs
Mast cells
Monocytes
T / NK
TNFSF9 TNFRSF9
TNFSF4 TNFRSF4
TNF TNFRSF1A
TNF ICOS
TNF FAS
IGF1 IGF1R
GMCSF GMCSFR
FAS FASLG
CXCL10 CXCR3
CD48 CD244
CD80 CD28
CCL2 CCR2
Control
Pro-inflam Macs
-log10(pvalue+1e-04)
log2 mean
B
NP
PE
57.69%
70.40%
IGF1
CD14
43.20%
67.65%
IGF1R
CD4
Frequency (%)
IGF1+CD14+ macrophages
IGF1R+CD4+ T cells
C
DMSO
Naive CD4+ T cells
BMS-754807
Coculture
PBS
Macrophages
EVs
D
DMSO
BMS-754807
PBS
NP-EVs
PE-EVs
PE-EVs
25.17%
34.03%
45.60%
30.98%
CCR7
CD45RO
CD45RO+CCR7+ CD4+ T cells (%)
7.34%
16.57%
26.30%
10.97%
IL-17A
CD4
CD4+ IL-17A+ T cells (%)
E
i.p. LPS (20μg/kg)
i.v. CD4+T cells
i.p. Anti-CD4 antibody
Euthanize
Embryonic day 0
10.5 11.5 12.5 15.5 18.5
F
LPS
PBS
PBS
Anti-CD4 antibody
PBS+DMSO
PBS+DMSO
PBS+DMSO
CD4+T cells+DMSO
CD4+T cells+BMS-754807
Embryo absorption rate (%)
Body weight of pups (g)
Crown-rump length of pups (mm)
G
Day10.5
Day16.5
Systolic Blood Pressure (mmHg)
Urine Albumin Creatine Ratio (μg/mg)
H
LPS
PBS
PBS
Anti-CD4 antibody
PBS+DMSO
PBS+DMSO
CD4+T cells+DMSO
CD4+T cells+BMS-754807
9.78%
22.74%
20.97%
10.58%
IL-17A
CD4
CD44+CD4+T cells (%)
CD44+CD4+IL-17A+ cells (%)
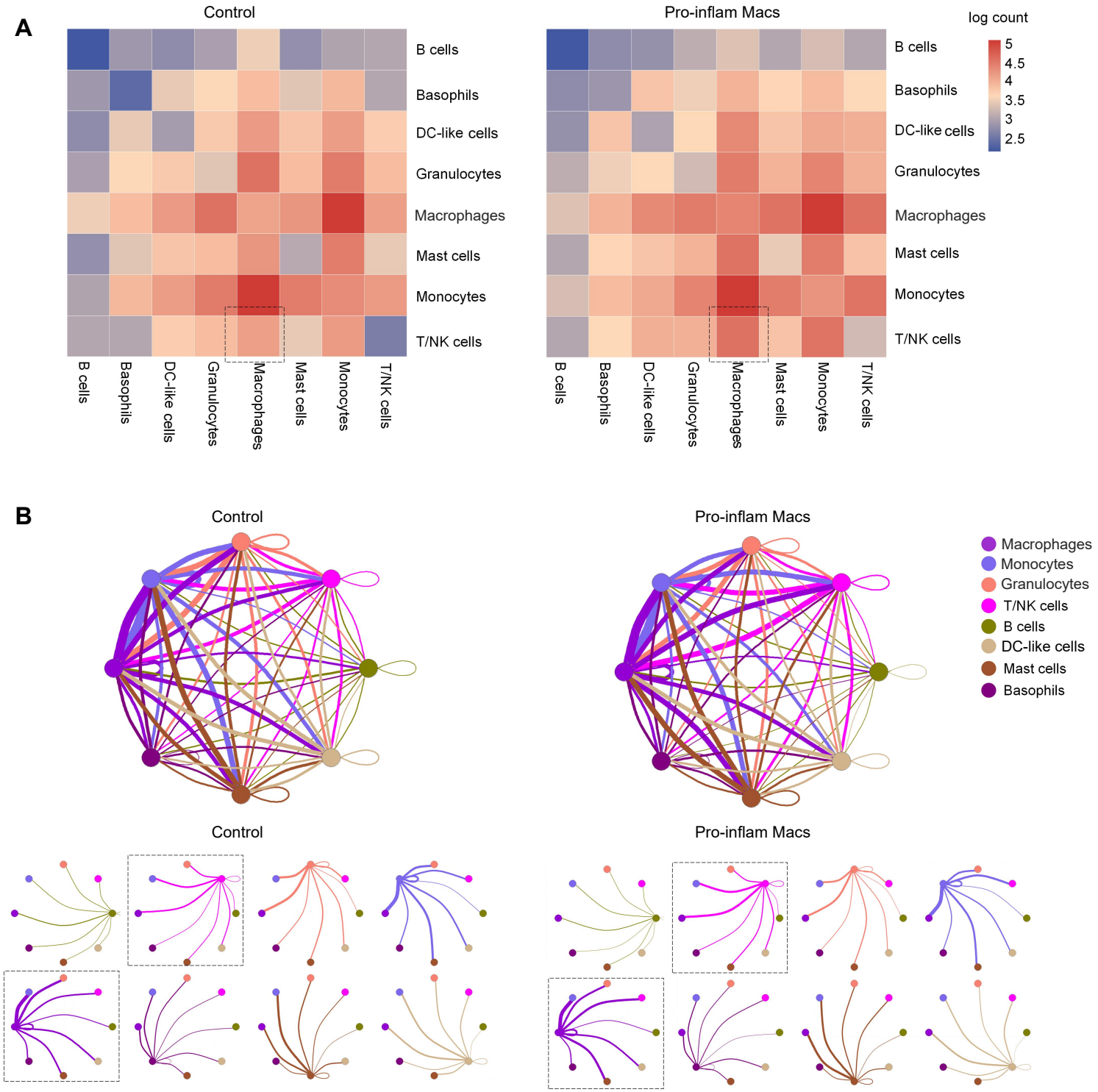
Figure 7 figure supplement 1